Author Manuscript

Author Manuscript

Author Manuscript

Author Manuscript

HHS Public Access

Author manuscript

Glia. Author manuscript; available in PMC 2023 December 01.

Published in final edited form as:

Glia. 2023 December ; 71(12): 2832–2849. doi:10.1002/glia.24454.

Pathological Bergmann glia alterations and disrupted calcium dynamics in ataxic Canavan disease mice

Vanessa L. Hull[1,2], **Yan Wang**[1,2], **Travis Burns**[1,2], **Sarah Sternbach**[3], **Shuaishuai Gong**[1,2], **Jennifer McDonough**[3], **Fuzheng Guo**[1,2], **Laura N. Borodinsky**[2,4], **David Pleasure**[1,2]

[1]Department of Neurology, University of California Davis School of Medicine, Sacramento, California, USA

[2]Institute for Pediatric Regenerative Medicine, Shriners Hospital for Children, Sacramento, California, USA

[3]Department of Biological Sciences, Kent State University, Kent, Ohio, USA

[4]Department of Physiology & Membrane Biology, University of California Davis School of Medicine, Sacramento, California, USA

Abstract

Canavan disease (CD) is a recessively inherited pediatric leukodystrophy resulting from inactivating mutations to the oligodendroglial enzyme aspartoacylase (ASPA). ASPA is responsible for hydrolyzing the amino acid derivative *N*-acetyl-L-aspartate (NAA), and without it, brain NAA concentrations increase by 50% or more. Infants and children with CD present with progressive cognitive and motor delays, cytotoxic edema, astroglial vacuolation, and prominent spongiform brain degeneration. ASPA-deficient CD mice (*Aspa*$^{nur7/nur7}$) present similarly with elevated NAA, widespread astroglial dysfunction, ataxia, and Purkinje cell (PC) dendritic atrophy. Bergmann glia (BG), radial astrocytes essential for cerebellar development, are intimately intertwined with PCs, where they regulate synapse stability, functionality, and plasticity. BG damage is common to many neurodegenerative conditions and frequently associated with PC dysfunction and ataxia. Here, we report that, in CD mice, BG exhibit significant morphological

This is an open access article under the terms of the Creative Commons Attribution-NonCommercial-NoDerivs License, which permits use and distribution in any medium, provided the original work is properly cited, the use is non-commercial and no modifications or adaptations are made.

Correspondence Vanessa L. Hull and David Pleasure, Institute for Pediatric Regenerative Medicine, UC Davis, c/o Shriners Hospital for Children, 2425 Stockton Blvd, Sacramento, CA 95817, USA. vhull@mednet.ucla.edu and depleasure@ucdavis.edu.

AUTHOR CONTRIBUTIONS

David Pleasure and Vanessa Hull conceived and designed the study. Vanessa Hull performed the immunohistochemistry, confocal imaging, morphological analyses and calcium imaging/analysis. Yan Wang performed the qPCR. Yan Wang and Vanessa Hull completed the cell culture experiments with help from Shuaishuai Gong. Fuzheng Guo provided required materials and guidance for qPCR and cell culture experiments. Laura Borodinsky designed the calcium imaging experiments and provided required materials and equipment. Sarah Sternbach and Jenny McDonough performed and analyzed NAA assays. Travis Burns performed rotarod testing. Vanessa Hull and David Pleasure wrote the manuscript. All authors reviewed and approved the manuscript.

Present address

Vanessa L. Hull, Department of Physiology, David Geffen School of Medicine, University of California, Los Angeles, Los Angeles, California, USA.

SUPPORTING INFORMATION

Additional supporting information can be found online in the Supporting Information section at the end of this article.

CONFLICT OF INTEREST STATEMENT

None.

Author Manuscript Author Manuscript Author Manuscript Author Manuscript

alterations, decreased structural associations with PCs, loss of synaptic support proteins, and altered calcium dynamics. We also find that BG dysfunction predates cerebellar vacuolation and PC damage in CD mice. Previously, we developed an antisense oligonucleotide (ASO) therapy targeting Nat8l (*N*-acetyltransferase-8-like, "Nat8l ASO") that inhibits the production of NAA and reverses ataxia and PC atrophy in CD mice. Here, we show that Nat8l ASO administration in adult CD mice also leads to BG repair. Furthermore, blocking astroglial uptake of NAA is neuroprotective in astroglia-neuron cocultures exposed to elevated NAA. Our findings suggest that restoration of BG structural and functional integrity could be a mechanism for PC regeneration and improved motor function.

Keywords

Bergmann glia; Canavan disease; astrocytes; astrocyte calcium; ataxia; cerebellum; Purkinje cell

1 | INTRODUCTION

Aspa mutations disrupting the function of the oligodendroglial-enriched enzyme aspartoacylase (ASPA) cause Canavan disease (CD), a neurodegenerative pediatric leukodystrophy (Matalon et al., 1988). The absence of ASPA-mediated cleavage of the abundant brain metabolite *N*-acetyl-L-aspartate (NAA) results in a significant elevation of brain NAA in CD patients (Baslow, 2000; Matalon et al., 1995). This manifests in infancy and early childhood as profound cognitive and motor impairments, seizures, astroglial vacuolation, and spongiform white matter degeneration (Hoshino & Kubota, 2014; Mendes et al., 2017). Similarly, CD mice ($Aspa^{nur7/nur7}$) present with elevated NAA, spongiform leukodystrophy, ataxia, and Purkinje cell (PC) damage (Hull et al., 2020; Traka et al., 2008).

Astrocytes are particularly damaged in CD, with CD mice exhibiting widespread astrogliosis and extensive astroglial vacuolation (Baslow & Guilfoyle, 2009). Moreover, astrocytes are the only parenchymal cell possessing a defined uptake mechanism for NAA: the sodium-coupled dicarboxylate transporter NaDC3 (encoded by *Slc13a3*; Fujita et al., 2005; Huang et al., 2000). Constitutive ablation of NaDC3 in CD mice protects against astroglial vacuolation and ataxia in CD mice (Wang, Hull, et al., 2021). Here, we focus on a specific subset of astrocytes, the Bergmann glia (BG), that undergo dramatic pathological changes in CD mice.

BG are radial astrocytes that direct the cytoarchitectural and functional development of the cerebellum, continuing to support neuronal survival and synaptic function throughout life. These specialized cells maintain their unipolar morphology and send their extensive processes through the molecular layer, terminating in subpial endfeet, which form the cerebellar glial limitans (Grosche et al., 2002; Rakic, 1971; Ramón y Cajal, 1909; Siegel et al., 1991). Much like the radial glial cells of the cerebral cortex, BG fibers act as a cerebellar scaffold that guides the migration of the dense excitatory granule cell (GC) population to their final destination (Hartmann et al., 1998; Rakic, 1971). BG also regulate the complex dendritic arborization of the PCs, inhibitory neurons that represent the sole motor output of the cerebellum (Bellamy, 2006; Lordkipanidze & Dunaevsky, 2005).

Author Manuscript Author Manuscript Author Manuscript Author Manuscript

During synaptogenesis, the previously smooth BG fibers form lateral projections that surround developing synapses in the molecular layer, forming glial microdomains (Grosche et al., 1999). BG microdomains will eventually enwrap both parallel fiber (PF)–PC synapses, which are the axonal inputs from the GCs, and climbing fiber (CF)–PC synapses (Bellamy, 2006; Grosche et al., 2002). The combined input from PFs and CFs modulates the inhibitory output of the PCs, influencing motor coordination, motor control, and learning (De Zeeuw & Hoogland, 2015). At these synapses, BG facilitate rapid glutamate reuptake mediated by glutamate transporters GLAST (glutamate aspartate transporter 1) and GLT1 (glutamate transporter 1; Bergles et al., 1997; Clark & Barbour, 1997; Rothstein et al., 1994; Storck et al., 1992). BG also regulate ion homeostasis (Wang et al., 2012) and sense and respond to both excitatory and inhibitory neurotransmission, the via expression of Ca^{2+}-permeable AMPARs (Burnashev et al., 1992; Saab et al., 2012), and $GABA_A$ receptors (Müller et al., 1994; Riquelme et al., 2002). Like all astrocytes, BG exhibit intracellular calcium fluctuations that can be spontaneous (Grosche et al., 1999) or evoked by synaptic activity (Hoogland et al., 2009).

Multiple animal models of BG ablation present with dysregulation of cerebellar neuronal migration, abnormal PC arborization, loss of motor coordination, and ataxia (Cui et al., 2001; Delaney et al., 1996), underscoring the vital role BG play in cerebellar development, information processing and functional output (De Zeeuw & Hoogland, 2015). PCs are also particularly susceptible to damage in cerebellar ataxias and recent studies show that BG alterations often accompany, and may even precede, PC damage (see Cerrato, 2020 for a comprehensive review of this topic). Here, in addition to describing complex alterations to BG and BG–PC structural associations in CD mice, we also show improvements to BG phenotypes after intracisternal delivery of an antisense oligonucleotide (ASO) previously shown to lower brain NAA and reverse leukodystrophy, ataxia and PC damage in CD mice (“Nat8l ASO,” Hull et al., 2020).

2 | MATERIALS AND METHODS

2.1 | Mice

Mice heterozygous for the *Aspa*^{nur7} nonsense mutation (RRID:IMSR_ JAX:008607) were maintained on a C57Bl/6J background and crossbred to generate *Aspa*$^{nur7/nur7}$ “CD mice” and sex and age-matched *Aspa*$^{WT/WT}$ controls (wild-type “[WT] mice”). Aldh1L1-eGFP (enhanced green flourescent protein) mice were also obtained from Jackson Laboratory (RRID:IMSR_JAX:030247) and crossbred to generate Aldh1L1-eGFP/*Aspa*$^{nur7/nur7}$ CD mice and sex and age-matched Aldh1L1-eGFP/*Aspa*$^{WT/WT}$ controls. For tissue harvest, mice were deeply anesthetized with ketamine/xylazine and transcardially perfused with cold phosphate-buffered saline. Cerebella were bisected sagittally and half was flash frozen for mRNA/biochemical assays and half was postfixed in 4% paraformaldehyde (PFA) in PBS, cryoprotected and embedded in optimal cutting temperature (OCT) compound and frozen. All animal experiments were conducted with the approval of the Institutional Animal Care and Use Committee of the University of California, Davis.

Author Manuscript Author Manuscript Author Manuscript Author Manuscript

2.2 | NAA assays

Brain NAA concentration was assayed by high-performance liquid chromatography (HPLC) (as described previously in Hull et al., 2020) and expressed in micromoles per gram tissue wet weight.

2.3 | Rotarod

Accelerating rotarod testing (4 rpm starting speed, increasing by 1.2 rpm every 10 s) was performed by blinded observers. Each data point represents the average score for an individual mouse over 9 trials.

2.4 | qRT/PCR

Total mRNA was isolated from cerebellar samples and assayed by quantitative real-time polymerase chain reaction (qRT-PCR). Results were normalized to *Hsp90* mRNA abundance. Primer pairs are detailed in Table 1.

2.5 | Cell culture

Whole brains were extracted from mice at postnatal days (p0–p2), followed by meticulous removal of the meninges. Subsequent enzymatic digestion was carried out using a mixture of papain (20 U/mL, Worthington) and DNase 1 (250 U/mL, Sigma) fortified with D-(+)-glucose (0.36%, AMRESCO) at 37°C for 60 min. The tissue was then mechanically triturated, resulting in a primary single-cell suspension (Wang, Hull, et al., 2021; Wang, Zhang, et al., 2021). Posttrituration, the cells were seeded on poly-D-lysine (Millipore) precoated cover glasses at a density of 5×10^5 cells/mL, in Dulbecco's Modified Eagle Medium supplemented with 10% heat-inactivated fetal bovine serum and a penicillin/streptomycin mix (all procured from ThermoFisher). On the subsequent *in vitro* day, the medium was further enhanced with 1 μm of cytarabino furanoside (AraC, C998100, TRC) for a duration of 24 h, to attenuate glial proliferation. Subsequently, medium was replenished with a fresh batch of coculture medium, with half-media changes implemented daily thereafter (Goshi et al., 2020; Hasan & Berdichevsky, 2021; Lesslich et al., 2022). On the seventh day, the coculture medium was augmented with varied concentrations of *N*-acetyl-L-asparate (NAA; 1, 2.5, and 10 mM) or a vehicle control, and this was maintained for an additional 2 days. Subsequently, the cells were fixed with 4% PFA for immunostaining.

2.6 | Immunostaining and image analysis

PFA-fixed (4%), OCT embedded, frozen cerebella were cryosectioned at 14 μm (slide mounted) or 50 μm (freefloating) and immunostained. Tissue sections and coculture coverslips were incubated with primary antibodies (Table 1) then incubated with secondary antibodies conjugated with fluorescent labels and counterstained with 4′,6-diamidino-2-phenylindole (DAPI). All imaging was done on a Nikon C2 laser scanning confocal microscope and consistent laser settings were used for all WT versus CD comparative images. Image analyses were performed in NIS-Elements (neuron and vacuolation quantification) or Imaris 9.7 (Bitplane, Zürich, Switzerland). Imaris was used to quantify BG process features (filament tracer), BG volume (surface tool), BG–PC proximity (surface tool with proximity filtering), VGLUT1/GluR4 mean fluorescence intensity (MFI; surface

Author Manuscript Author Manuscript Author Manuscript Author Manuscript

tool), and VGLUT2 puncta per PC (spots tool). For Aldh1L1-eGFP/vimentin volume quantification, ROIs included the molecular layer and the PC layer but not the granular layer. All other ROIs included only the molecular layer, excluding both the granular layer and PC layer.

2.7 | Calcium imaging

Mice (p20–p30) were deeply anesthetized with ketamine/xylazine and cerebella were vibratome-sectioned at 250 μm ice cold-cutting solution. Cutting solution consisted of 75 mM sucrose, 87 mM NaCl, 25 mM Glucose, 25 mM $NaHCO_3$, 7 mM $MgCl_2$, 2.5 mM KCl, 1.25 mM NaH_2PO_4, 0.5 mM $CaCl_2$, bubbled with 5% CO_2/95%O_2. Slices were then incubated in 1 μm sulforhodamine 101 (SR101, Invitrogen) in artificial cerebrospinal fluid (aCSF) for 20 min, followed by aCSF alone for 10 minutes, both at 34°C bubbling with 5% CO_2/95%O_2. aCSF solution consisted of 125 mM NaCl, 25 mM Glucose, 25 mM $NaHCO_3$, 7 mM $MgCl_2$, 2.5 mM KCl, 1.25 NaH_2PO_4, and 2 mM $CaCl_2$: ~300 mOsm. Slices were then incubated in 5 μM Fluo4-AM (ThermoFisher Scientific) in aCSF at room temperature for 45 min, then washed in aCSF before being time-lapse imaged by a Swept-Field confocal microscope (Nikon) at an acquisition rate of 5 Hz for 5 min. After spontaneous recordings were performed, the same slices were treated with 0.3 μm AMPA just prior to image acquisition. Videos were analyzed using NIS Elements to measure Fluo4-AM+ transients in SR101+ BG processes in the molecular layer. Fluorescence intensity (in arbitrary units, AU) for sample traces was quantified as $\Delta F/F_0$ with F_0 being average baseline intensity. Number of transients per minute over a 5-min recording window in an 1000 μm^3 region of interest (ROI) were averaged for each animal so that each data point represents the average of three ROIs (each from a different slice) for one animal. Duration of transients is reported in seconds (s) with each data point representing the average transient duration or rise time duration during a 5-min recording window in a single BG cell microdomain ($n = 4$ mice per group).

2.8 | Nat8l ASO therapy

A locked nucleic acid antisense oligonucleotide (“LNA-ASO,” Smith & Zain, 2019) designed by Qiagen to knockdown Nat8l expression (“Nat8l ASO,” nucleotide sequence GGCGTAGAGCAGTTGG) and a negative control LNA-ASO with no known eukaryote targets (“control ASO,” nucleotide sequence AACACGTCTATACGC) were injected intracisternally into 2-month-old sex-matched WT or CD Mice (0.5 nmol in 5 μL of aCSF, rate of 1 μL/min; under isoflurane anesthesia). Brain tissue was harvested for analysis at 7, 14 days, and 2 months posttreatment. For full details, refer to Hull et al. (2020).

2.9 | Statistics

Quantitative data are presented in the figures as means ± SEM. Statistical analyses were done by two-tailed, unpaired student's *t*-test (with Bonferroni correction for multiple comparisons where appropriate) or one- or two-way analysis of variance (ANOVA) with post hoc Tukey's test as indicated in figure legends.

Author Manuscript Author Manuscript Author Manuscript Author Manuscript

3 | RESULTS

"CD mice" homozygous for the *Aspa*^{nur7} nonsense mutation have no detectable ASPA by Western blot assays (Traka et al., 2008) and exhibit marked overaccumulation of NAA in brain tissue (Figure 1a). CD mice exhibit prominent astroglial and intramyelinic vacuolation and astrogliosis throughout the brain by postnatal day (p30), quantified in Figure 1b and visible in images of cerebellar (Figure 1c, left panel) and thalamic (Figure 1c, right panel) white matter. CD mice have lower rotarod retention times compared with age- and sex-matched WT mice in maturity (Figure 1d). No obvious CD-related phenotypic differences have been reported in CD mice on the basis of sex. Indeed, NAA levels, rotarod performance, and therapeutic responses are similar in male and female mice (Hull et al., 2020).

There is significant disruption to the morphology of BG of the cerebellum in adult CD mice, characterized by fragmented and irregular processes that lose linearity and exhibit swelling. These changes are visualized in tissue sections derived from transgenic mice that express GFP under the aldehyde dehydrogenase 1 family member L1 (*Aldh1L1*) promoter (Aldh1L1-eGFP mice; Doyle et al., 2008) that have been coimmunolabeled for the BG cytoskeletal marker vimentin (Figure 2a,b). Expression of calcium binding protein S100β is reduced in BG somata and processes in CD mice (Figure 2c). Volumetric analysis performed in Imaris 9.7 (Bitplane) reveals that CD mice have more total Aldh1L1-eGFP volume per BG (Figure 2d) and total vimentin volume per BG (Figure 2e). Next, we utilized the filament tracing tool in Imaris to isolate and measure features specific to vimentin+ BG processes in the molecular layer. BG processes in CD mice have a higher volume than WT mice (Figure 2f). Furthermore, as outlined in the graphic in Figure 2g, there are a higher number of segments per BG (Figure 2h), terminal points per BG (Figure 2i), and a higher number of branches per BG process (Figure 2i) in CD mice as compared with WT mice.

We previously reported a substantial diminution in dendritic length and spine density in PCs in CD mice (Hull et al., 2020). In conjunction with PC simplification, we find major disruptions to BG cell morphology, BG soma are irregularly shaped, dislocated from their natural position, and exhibit decreased SOX2 expression in CD mice (Figure 3a). Vimentin+ BG processes are enlarged, fractured, and/or absent in large swaths from areas where calbindin+ PC dendrites are simplified and/or missing in CD mice (Figure 3a,b). These features are in marked contrast to WT BG processes, which exhibit a more consistent diameter and even spacing throughout the molecular layer where they are intricately interwoven with complex PC dendritic arborization (Figure 3a,b). Aldh1L1-eGFP signal from BG cell bodies in the PC layer of CD mice is irregular with hypo- and hyperintense regions, compared with the consistent signal present in WT mice (Figure 3b). We generated 3D reconstructions of confocal images in Imaris which allows for proximity analysis between Aldh1L1-eGFP+/vimentin+ BG and calbindin+ PCs. The results reveal that a lower percentage of Aldh1L1-eGFP and vimentin signal, respectively, are within 1 μ of PC marker calbindin in CD mice (Figure 3c,d). Taken together, these data demonstrate a significant reduction in BG–PC structural associations in the CD cerebellum.

Author Manuscript Author Manuscript Author Manuscript Author Manuscript

We reasoned that the dissociation of BG and PC could result in the loss of synaptic contacts between the PFs of the excitatory GCs and PC dendrites, synapses which are typically enwrapped and supported by BG microdomains. Coinciding with irregular BG and PC morphology in CD mice (Figure 4a, top and bottom panels), immunostaining for vesicular glutamate transporter 1 (VGLUT1) + PF–PC synapses reveals a marked reduction of signal in CD mice (Figure 4b,b') as compared with WT mice (Figure 4a,a'), quantified by MFI (Figure 4c). PCs also receive synaptic input from VGLUT2+ CF. CD mice exhibit a visible decrease in VGLUT2+ CF terminals in the molecular layer (Figure 4e,e',f,f'), which we quantified in Imaris by counting the number of VGLUT2+ puncta per cell in the molecular layer (Figure 4d).

Given the loss of BG–PC proximity and PF–PC/CF–PC synapses in the molecular layer, we decided to explore other features of BG microdomains that could also be disrupted in CD. BG microdomains highly express AMPARs with a subunit composition unique in the molecular layer: lack of GluR2 with expression of GluR1 and GluR4 subunits, encoded by *GluA2, GluA1*, and *GluA4*, respectively. This configuration confers calcium permeability in the presence of glutamate (Burnashev et al., 1992; Keinänen et al., 1990; Müller et al., 1992; Saab et al., 2012). We therefore used GluR4 as a marker for BG Ca^{2+}-permeable AMPARs and observed a visible decrease in GluR4 protein level in the molecular layer of CD mice by immunohistochemistry (Figure 5a) which matches the decreased level of GluR4 MFI (Figure 5b). *GluA4* message level in whole cerebellar tissue of CD mice is lower than in WT (Figure 5c). BG processes also abundantly express glutamate transporters GLAST and, to a lesser extent, GLT-1, which have demonstrated roles in glutamate reuptake (Bergles et al., 1997). We find that CD mice exhibit a decrease in GLAST protein level visible by IHC (Figure 5d) in the molecular layer as well as a decrease in total cerebellar *Slc1a3* (encodes GLAST, Figure 5e) and *Slc1a2* (encodes GLT-1, Figure 5f) mRNA. In sum, we find that BG in CD mice demonstrate significant losses to synapse-supporting microdomain proteins.

Next, we sought to determine the age at which cerebellar cellular abnormalities first arise in CD mice. At p7, immature PCs (Figure S1a) and BG (Figure S1a,b) appear similar in WT and CD mice. However by p14, a marginal increase in vimentin immunoreactivity becomes observable in BG processes of CD mice (Figure S1c,d). By p21, BG irregularities and PC dendritic abnormalities are clearly visible in CD mice (Figure S1e,f,f'), worsening by p30 (Figure S1g,h,h'). BG processes in p21 CD mice are swollen, particularly in distal regions, and exhibit irregular lateral protuberances, while somas also begin to take on the asymmetrical shape seen in adult CD mice (Figure S1e,f,f',g,g'). PCs in CD mice at p21 (Figure S1e) and p30 (Figure S1g) exhibit less complex dendritic branching and show a less continuous relationship with BG processes, consistent with our findings in more mature mice (Figure 3).

Ataxic gait is observed in CD mice as early as the second postnatal week however extensive vacuolation is not observed throughout the brain until p21 (Traka et al., 2008). Therefore, we decided to further characterize the onset of vacuolation in addition to BG–PC abnormalities during this newly defined critical p14–p21 window. Cerebellar white matter appears consistent in WT and CD mice at p15 (Figure 6a). However, BG show signs of irregularity at these early timepoints, including decreased SOX2 signal in soma (Figure 6b),

Author Manuscript Author Manuscript Author Manuscript Author Manuscript

more intense/irregular aldh1l1-eGFP expression and increased glial fibrillary acid protein (GFAP) immunoreactivity (Figure 6c). PC morphology, however, appears similar between WT and CD mice at p15 (Figure 6b).

Based on these findings, we hypothesized that BG could be a noncell autonomous mechanism for PC dysfunction in CD, Prior *in vitro* studies have demonstrated that neurons do not take up NAA (Sager et al., 1999) and elevated NAA is not neurotoxic to neurons in culture or slice preparations and does not alter electrophysiological properties of neurons (Appu et al., 2017; Kolodziejczyk et al., 2009; von Jonquieres et al., 2018). Astrocytes, however, readily take up NAA in culture (Sager et al., 1999) via the sodium-coupled NAA transporter NaDC3 (encoded by *Slc13a3*; Fujita et al., 2005). Single-cell sequencing data (Kozareva et al., 2021) and IHC confirm the expression of NaDC3 in BG (Figure 7a). In prior work, we have shown that constitutive ablation of NaDC3 also expressed in the meninges and kidney, protects against astroglial vacuolation and ataxia in CD mice (Wang, Hull, et al., 2021). To investigate the potential influence of astrocytes on neuronal survival in the context of CD, we cocultured primary neurons and astrocytes in the presence of increasing concentrations of NAA. We found that neuronal survival was significantly reduced at 1 mM and higher concentrations of NAA in WT cultures (Figure 7b,c). However, when the astroglial uptake of NAA was blocked by constitutive NaDC3 ablation (in cultures derived from *Slc13a3*$^{-/-}$ mice, Figure 7b,d), there was no significant effect on neuronal survival at 1 or 2.5 mM concentrations of NAA.

To better understand the functional implications of the pathological changes we observe in BG in CD mice, we performed imaging using the calcium indicator Fluo4-AM in acute cerebellar slice preparations. We procured slices from mice aged p21–p30 when, as we have established, BG alterations are already present. In addition to broad full-cell and multicell spanning calcium waves, we observed spontaneously occurring compartmentalized calcium transients that colocalized with astrocyte-specific dye SR101 (Nimmerjahn et al., 2004) in BG processes (Figure 8a). Recorded calcium transients were ~1–2 μ wide and appear consistent with signals observed in BG by others acute slice preparations (Beierlein & Regehr, 2006; Burnashev et al., 1992; Grosche et al., 1999) and in SR101-loaded BG processes during *in vivo* calcium imaging (Nimmerjahn et al., 2009; Figure 8b,c). We recorded a significantly lower frequency of spontaneous calcium transients in CD mice compared with WT (Figure 8d). The duration of these events is also significantly prolonged in CD mice (Figure 8e), while the rise time remains similar to that of WT mice (Figure 8f). After recording spontaneous transients, slices were treated with AMPA. AMPA-evoked transients exhibit similar kinetics to spontaneous calcium transients in BG in WT samples, while in CD mice, the duration of AMPA-evoked transients was longer (Figure 8e,f). Overall, we find that BG in CD mice exhibit less spontaneous calcium activity and the duration of spontaneous or AMPA-evoked single events is prolonged with no change in rise time.

We previously developed an ASO targeting the knockdown of the NAA-synthesizing enzyme NAT8L (“Nat8l ASO”) with the prediction that decreasing elevated levels of brain NAA would be therapeutic for CD mice. Intracisternal delivery of this Nat8l ASO to adult, symptomatic CD mice reversed spongiform vacuolation and ataxia within 2 weeks of

Author Manuscript Author Manuscript Author Manuscript Author Manuscript

treatment and repaired PC dendritic atrophy leading to an increase in PC spine density (Hull et al., 2020). We questioned whether BG damage was also reversible with this treatment and indeed, BG in Nat8l ASO-treated mice exhibit more intact morphology than untreated controls (Figure 9a). Treatment also results in an increase in GluR4 immunostaining (Figure 9b) and GluR4 MFI (Figure 9c) in the molecular layer of Nat8l ASO-treated CD mice (30 days posttreatment) when compared with untreated CD mice or CD mice treated with a control ASO with no known eukaryotic targets ("Ctrl-ASO"). These data correspond with an increase in *GluA4* transcript (encoding GluR4) which climbs to WT levels by 60 days postadministration (Figure 9d). The transcript levels of *Slc1a3* (Figure 9e) and *Slc1a2* (Figure 9f), encoding GLAST and GLT-1, respectively, progressively increase over time in Nat8l ASO-treated CD mice, ultimately also reaching WT levels. In summary, we find that Nat8l ASO therapy improves BG morphology and increases BG microdomain protein expression in CD mice.

4 | DISCUSSION

The hallmark of CD is elevated brain NAA which, in the absence of functional ASPA, results in widespread astroglial dysfunction, demonstrated here in BG of CD mice. NAA is elevated throughout the brain by p21 in CD mice, with the highest NAA concentration found in the cerebellum (Traka et al., 2008). Here we show that BG dysfunction present at p15–p17 coincides with the first signs of motor disturbances in CD mice and importantly, these features predate widespread vacuolation and PC abnormalities seen at p21.

Astrocytes, including BG, express the sodium-coupled dicarboxylic acid transporter NaDC3 (encoded by *Slc13a3*) making them the only parenchymal cell type with the ability to take up NAA (Bergeron et al., 2013; Fujita et al., 2005; Huang et al., 2000). We hypothesize that NaDC3-mediated overloading of astroglia with NAA and sodium causes osmolar dysregulation and vacuolation in CD mice. In prior work, we demonstrated that constitutive deletion of NaDC3 prevents leukodystrophy, astroglial vacuolation, and ataxia in CD mice (Wang, Hull, et al., 2021; Wang, Zhang, et al., 2021). Here, we show that in the presence of high NAA, primary neurons cocultured with NaDC3-deficient astrocytes have enhanced survivability versus WT astrocytes. BG, as specialized astrocytes, also have *Slc13a3* transcript (Kozareva et al., 2021) and NaDC3 protein. Moreover, when ASPA-deficient mice are supplanted with astroglial ASPA only, the CD phenotype is reversed (Gessler et al., 2017), providing further support that astroglial-NAA overloading may be an essential catalyst in the pathophysiology of CD.

The compromised structural integrity of BG and retraction of BG processes from PC dendrites may be the underlying cause of PC simplification and PF–/CF–PC synaptic loss in CD mice. PFs influence simple spike firing in PCs and play important roles in locomotion, motor coordination, and motor learning (Galliano et al., 2013; Hoogland et al., 2015; Vinueza Veloz et al., 2015), while CF input drives complex spikes, helping with movement adjustment and fine motor coordination. CF and PF inputs to PCs are both critical for motor learning and adaptation (Ito, 2002, 2006). We show that BG irregularities predate PF–PC synaptogenesis and coincide with the final stages of CF pruning (Crepel et al., 1976; Hashimoto & Kano, 2013), BG differentiation is temporally and functionally correlated

Author Manuscript Author Manuscript Author Manuscript Author Manuscript

with PC dendritic outgrowth and synaptogenesis in the molecular layer occurring around the second postnatal week (Yamada & Watanabe, 2002). PF–PC synaptic dysfunction is common in several mouse models of ataxia (including the ATXN1 mouse model for spinocerebellar ataxia; Barnes et al., 2011; Ebner et al., 2013; Hoxha et al., 2016; Koeppen, 2005; Smeets et al., 2021; Zuo et al., 1997) and frequently observed in conjunction with BG dysfunction (Burright et al., 1995; Custer et al., 2006; Shiwaku et al., 2013). Disruption of CF–PC synapses is seen in postmortem tissue from patients with spinocerebellar ataxias, Parkinson's disease, and essential tremor (Koeppen, 2005; Kuo et al., 2017; Lin et al., 2014).

BG express glutamate transporters GLAST and GLT-1 that facilitate glutamate reuptake, thereby shaping the time course of postsynaptic receptor activation (Bergles et al., 1997; Dzubay & Jahr, 1999; Takahashi et al., 1996). GLAST and GLT-1 also protect against extrasynaptic glutamate spillover (Brasnjo & Otis, 2001; Reichelt & Knöpfel, 2002), prevent excitotoxicity due to prolonged glutamate elevation (Meldrum & Garthwaite, 1990), and decrease the activation of AMPARs on PCs at PF–PC synapses during repeated stimulation (Marcaggi et al., 2003). GLAST-null mice exhibit disturbances in PF–PC synapses (Miyazaki et al., 2017), neuronal atrophy (Rothstein et al., 1996), and motor discoordination (Watase et al., 1998), all of which are phenotypes we have now documented in CD mice. GLAST loss is evident in multiple spinocerebellar ataxias (Lin et al., 2000; Perkins et al., 2010), Alzheimer's disease (Sjöbeck & Englund, 2001), and more specifically, BG GLAST depletion in ATXN1 mice has been associated with PC loss (Cvetanovic, 2015).

In addition to glutamate transporters, BG microdomains also feature Ca^{2+}-permeable AMPARs, unique in the molecular layer for their GluR1/GluR4-subunit composition. These Ca^{2+}-permeable AMPARs within BG exhibit a relatively high Ca^{2+} conductance even in low Ca^{2+} (Burnashev et al., 1992) and Ca^{2+} entry results in a robust reduction in the resting BG potassium conductance (Müller et al., 1992). Ca^{2+} influx through these AMPARs is considered the primary mechanism by which BG can “sense” functional synapses when they first become active (Bellamy, 2006; Iino et al., 2001). Selectively deleting BG AMPARs or blocking their Ca^{2+} permeability triggers retraction of BG processes from PC synapses (Iino et al., 2001; Saab et al., 2012), increasing the amplitude and duration of PC currents, delaying glutamatergic synapse formation and impairing fine motor coordination in developing mice (Saab et al., 2012). Conversely, overexpression of BG AMPARs drives the extension and overgrowth of BG processes (Ishiuchi et al., 2001). BG AMPARs are therefore not only crucial for regulating the structural and functional establishment of microdomains during development, but they are also integral to synaptic stability and axonal outgrowth in adults.

We also observed a reduction in spontaneous Ca^{2+} activity and an increase in the total duration, but not the rise time, of BG spontaneous and AMPA-stimulated localized Ca^{2+} transients in BG of CD mice. The Ca^{2+} transients we recorded are consistent with spontaneous and PF-stimulation-induced signals isolated to BG microdomains in cerebellar slices (Beierlein & Regehr, 2006; Grosche et al., 1999) and “calcium sparkles” reported by (Nimmerjahn et al., 2009) during *in vivo* calcium imaging of awake, behaving mice. PF and/or CF stimulation reliably produces localized calcium transients in BG (Beierlein & Regehr, 2006; Grosche et al., 1999; Hoogland et al., 2009; Matsui & Jahr, 2004),

Author Manuscript Author Manuscript Author Manuscript Author Manuscript

therefore the AMPA-evoked Ca^{2+} fluctuations we observed in BG potentially result from the combined influence of Ca^{2+} entry through BG Ca^{2+}-permeable AMPARs and activation of metabotropic glutamate receptor 1/purinergic receptors which triggers IPR3-mediated calcium release from internal stores.

The implications of the loss of spontaneous BG activity and prolonged intracellular calcium elevation we observed in CD mice are widespread (see Shigetomi et al., 2016 for a review of calcium signaling in astrocytes). Using optogenetic stimulation, Sasaki et al. (2012) showed that increased intracellular calcium in BG induces glutamate release, activates AMPARs on PCs, induces LTD in PF–PC synapses, and ultimately leads to disturbances in associative motor learning and/or motor performance of cerebellar mediated behaviors. K^+ uptake by BGs is a Ca^{2+}-dependent processes known to regulate PC membrane potential and PCs show an increase in spike activity when extracellular K^+ is depleted due to increased BG Ca^{2+} signaling in acute slices and in vivo (Wang et al., 2012). Activation of BG AMPARs also strongly inhibits BG–BG gap junctional coupling (Müller et al., 1996) and increased intracellular Ca^{2+} in astrocytes has been shown to elevate intracellular calcium in neighboring neurons (Nedergaard, 1994; Parpura et al., 1994).

The integral roles that BG play in cerebellar structural and functional development are highly evident given the strong phenotypes associated with BG dysregulation and damage, many of which have been demonstrated here in CD mice. BG actively participate in cerebellar information processing by regulating synaptogenesis and supporting synaptic activity, indirectly via ion buffering and careful shaping of the glutamate curve, and/or directly via calcium signaling, glutamate release, and upstream activation of LTD pathways at PF–PC synapses (De Zeeuw & Hoogland, 2015). Our results indicate disruptions to all of these functions in CD mice. Our results also indicate that astroglial overloading with NAA via NaDC3 can damage neuronal health *in vitro*. Furthermore, ataxia predates cerebellar vacuolation in CD mice, coinciding instead with early BG abnormalities. Given the intimate relationship between BG and PCs, and the significant dependence of PC on BG for synaptic development, stability, and ongoing support, BG damage may potentially represent a noncell autonomous mechanism of PC degeneration in CD. We are encouraged by our findings that many of the BG alterations seen in CD mice are improved by Nat8l ASO therapy. Overall, our findings point to early disruptions to BG integrity and dysregulation of the BG–PC relationship as a driver for CD pathogenesis and warrant further investigation into potential therapeutic targets for BG repair in CD and other neurological diseases.

Supplementary Material

Refer to Web version on PubMed Central for supplementary material.

ACKNOWLEDGMENTS

This study was supported by the National Center for Advancing Translational Sciences, National Institutes of Health, through grant number UL1 TR001860 and linked award TL1 TR001861 (Vanessa L. Hull), National Science Foundation grant 1754340 (Laura N. Borodinsky), National Institutes of Health grants: R01NS123080, R01NS123165, and R21NS125464 (Fuzheng Guo), R01NS105886 and R01NS113859 (Laura N. Borodinsky), R21NS117386 and R21NS13381 (David Pleasure), and funds from the Shriners Hospitals for Children. We would

Author Manuscript Author Manuscript Author Manuscript Author Manuscript

like to thank Dr. Marco González for comments on the article. Parts of the graphical abstract were created with BioRender.com.

Funding information

National Center for Advancing Translational Sciences; National Institutes of Health, Grant/Award Numbers: R21NS13381, R21NS117386, R01NS113859, R01NS105886, R21NS125464, R01NS123165, R01NS123080, TL1 TR001861, UL1 TR001860; National Science Foundation, Grant/Award Number: 1754340; Shriners Hospitals for Children

DATA AVAILABILITY STATEMENT

The data that support the findings of this study are available from the corresponding authors upon reasonable request.

REFERENCES

Appu AP, Moffett JR, Arun P, Moran S, Nambiar V, Krishnan JKS, Puthillathu N, & Namboodiri AMA (2017). Increasing N-acetylaspartate in the brain during postnatal myelination does not cause the CNS pathologies of Canavan disease. Frontiers in Molecular Neuroscience, 10, 161. 10.3389/fnmol.2017.00161 [PubMed: 28626388]

Barnes JA, Ebner BA, Duvick LA, Gao W, Chen G, Orr HT, & Ebner TJ (2011). Abnormalities in the climbing fiber-Purkinje cell circuitry contribute to neuronal dysfunction in ATXN1[82Q] mice. Journal of Neuroscience, 31(36), 12778–12789. 10.1523/JNEUROSCI.2579-11.2011 [PubMed: 21900557]

Baslow MH (2000). Canavan's spongiform leukodystrophy: A clinical anatomy of a genetic metabolic CNS disease. Journal of Molecular Neuroscience, 15(2), 61–70. 10.1385/JMN:15:2:61 [PubMed: 11220786]

Baslow MH, & Guilfoyle DN (2009). Are astrocytes the missing link between lack of brain aspartoacylase activity and the spongiform leukodystrophy in Canavan disease? Neurochemical Research, 34(9), 1523–1534. 10.1007/s11064-009-9958-z [PubMed: 19319678]

Beierlein M, & Regehr WG (2006). Brief bursts of parallel fiber activity trigger calcium signals in Bergmann glia. Journal of Neuroscience, 26(26), 6958–6967. 10.1523/JNEUROSCI.0613-06.2006 [PubMed: 16807325]

Bellamy T (2006). Interactions between Purkinje neurones and Bergmann glia. The Cerebellum, 5(2), 116–126. 10.1080/14734220600724569 [PubMed: 16818386]

Bergeron MJ, Clémençon B, Hediger MA, & Markovich D (2013). SLC13 family of Na+-coupled di- and tri-carboxylate/sulfate transporters. Molecular Aspects of Medicine, 34(2), 299–312. 10.1016/j.mam.2012.12.001 [PubMed: 23506872]

Bergles DE, Dzubay JA, & Jahr CE (1997). Glutamate transporter currents in Bergmann glial cells follow the time course of extrasynaptic glutamate. Proceedings of the National Academy of Sciences of the United States of America, 94(26), 14821–14825. 10.1073/pnas.94.26.14821 [PubMed: 9405697]

Brasnjo G, & Otis TS (2001). Neuronal glutamate transporters control activation of postsynaptic metabotropic glutamate receptors and influence cerebellar long-term depression. Neuron, 31(4), 607–616. 10.1016/s0896-6273(01)00377-4 [PubMed: 11545719]

Burnashev N, Khodorova A, Jonas P, Helm PJ, Wisden W, Monyer H, Seeburg PH, & Sakmann B (1992). Calcium-permeable AMPA-Kainate receptors in fusiform cerebellar glial cells. Science, 256(5063), 1566–1570. [PubMed: 1317970]

Burright EN, Brent Clark H, Servadio A, Matilla T, Feddersen RM, Yunis WS, Duvick LA, Zoghbi HY, & Orr HT (1995). SCA1 transgenic mice: A model for neurodegeneration caused by an expanded CAG trinucleotide repeat. Cell, 82(6), 937–948. 10.1016/0092-8674(95)90273-2 [PubMed: 7553854]

Cerrato V. (2020). Cerebellar astrocytes: Much more than passive bystanders In ataxia pathophysiology. Journal of Clinical Medicine, 9(3), E757. 10.3390/jcm9030757

Author Manuscript Author Manuscript Author Manuscript Author Manuscript

Clark BA, & Barbour B (1997). Currents evoked in Bergmann glial cells by parallel fibre stimulation in rat cerebellar slices. The Journal of Physiology, 502(Pt 2), 335–350. 10.1111/j.1469-7793.1997.335bk.x [PubMed: 9263914]

Crepel F, Mariani J, & Delhaye-Bouchaud N (1976). Evidence for a multiple innervation of Purkinje cells by climbing fibers in the immature rat cerebellum. Journal of Neurobiology, 7(6), 567–578. 10.1002/neu.480070609 [PubMed: 1003202]

Cui W, Allen ND, Skynner M, Gusterson B, & Clark AJ (2001). Inducible ablation of astrocytes shows that these cells are required for neuronal survival in the adult brain. Glia, 34(4), 272–282. 10.1002/glia.1061 [PubMed: 11360300]

Custer SK, Garden GA, Gill N, Rueb U, Libby RT, Schultz C, Guyenet SJ, Deller T, Westrum LE, Sopher BL, & la Spada AR (2006). Bergmann glia expression of polyglutamine-expanded ataxin-7 produces neurodegeneration by impairing glutamate transport. Nature Neuroscience, 9(10), 1302–1311. 10.1038/nn1750 [PubMed: 16936724]

Cvetanovic M. (2015). Decreased expression of glutamate transporter GLAST in Bergmann glia is associated with the loss of Purkinje neurons in the spinocerebellar ataxia type 1. Cerebellum (London, England), 14(1), 8–11. 10.1007/s12311-014-0605-0 [PubMed: 25255716]

De Zeeuw CI, & Hoogland TM (2015). Reappraisal of Bergmann glial cells as modulators of cerebellar circuit function. Frontiers in Cellular Neuroscience, 9, 246. 10.3389/fncel.2015.00246 [PubMed: 26190972]

Delaney CL, Brenner M, & Messing A (1996). Conditional ablation of cerebellar astrocytes in postnatal transgenic mice. The Journal of Neuroscience, 16(21), 6908–6918. [PubMed: 8824329]

Doyle JP, Dougherty JD, Heiman M, Schmidt EF, Stevens TR, Ma G, Bupp S, Shrestha P, Shah RD, Doughty ML, Gong S, Greengard P, & Heintz N (2008). Application of a translational profiling approach for the comparative analysis of CNS cell types. Cell, 135(4), 749–762. 10.1016/j.cell.2008.10.029 [PubMed: 19013282]

Dzubay JA, & Jahr CE (1999). The concentration of Synaptically released glutamate outside of the climbing fiber–Purkinje cell synaptic cleft. Journal of Neuroscience, 19(13), 5265–5274. 10.1523/JNEUROSCI.19-13-05265.1999 [PubMed: 10377338]

Ebner BA, Ingram MA, Barnes JA, Duvick LA, Frisch JL, Clark HB, Zoghbi HY, Ebner TJ, & Orr HT (2013). Purkinje cell Ataxin-1 modulates climbing fiber synaptic input in developing and adult mouse cerebellum. Journal of Neuroscience, 33(13), 5806–5820. 10.1523/JNEUROSCI.6311-11.2013 [PubMed: 23536093]

Fujita T, Katsukawa H, Yodoya E, Wada M, Shimada A, Okada N, Yamamoto A, & Ganapathy V (2005). Transport characteristics of N-acetyl-L-aspartate in rat astrocytes: Involvement of sodium-coupled high-affinity carboxylate transporter NaC3/NaDC3-mediated transport system. Journal of Neurochemistry, 93(3), 706–714. [PubMed: 15836629]

Galliano E, Gao Z, Schonewille M, Todorov B, Simons E, Pop AS, D'Angelo E, van den Maagdenberg AMJM, Hoebeek FE, & de Zeeuw CI (2013). Silencing the majority of cerebellar granule cells uncovers their essential role in motor learning and consolidation. Cell Reports, 3(4), 1239–1251. 10.1016/j.celrep.2013.03.023 [PubMed: 23583179]

Gessler DJ, Li D, Xu H, Su Q, Sanmiguel J, Tuncer S, Moore C, King J, Matalon R, & Gao G (2017). Redirecting N-acetylaspartate metabolism in the central nervous system normalizes myelination and rescues Canavan disease. JCI Insight, 2(3), e90807. 10.1172/jci.insight.90807 [PubMed: 28194442]

Goshi N, Morgan RK, Lein PJ, & Seker E (2020). A primary neural cell culture model to study neuron, astrocyte, and microglia interactions in neuroinflammation. Journal of Neuroinflammation, 17(1), 155. 10.1186/s12974-020-01819-z [PubMed: 32393376]

Grosche J, Kettenmann H, & Reichenbach A (2002). Bergmann glial cells form distinct morphological structures to interact with cerebellar neurons. Journal of Neuroscience Research, 68(2), 138–149. 10.1002/jnr.10197 [PubMed: 11948659]

Grosche J, Matyash V, Möller T, Verkhratsky A, Reichenbach A, & Kettenmann H (1999). Microdomains for neuron–glia interaction: Parallel fiber signaling to Bergmann glial cells. Nature Neuroscience, 2(2), 139–143. 10.1038/5692 [PubMed: 10195197]

Author Manuscript Author Manuscript Author Manuscript Author Manuscript

Hartmann D, Schulze M, & Sievers J (1998). Meningeal cells stimulate and direct the migration of cerebellar external granule cells in vitro. Journal of Neurocytology, 27(6), 395–409. 10.1023/A:1006998609999 [PubMed: 10192521]

Hasan MF, & Berdichevsky Y (2021). Neuron and astrocyte aggregation and sorting in three-dimensional neuronal constructs. Communications Biology, 4(1), 587. 10.1038/s42003-021-02104-2 [PubMed: 34002005]

Hashimoto K, & Kano M (2013). Synapse elimination in the developing cerebellum. Cellular and Molecular Life Sciences, 70(24), 4667–4680. 10.1007/s00018-013-1405-2 [PubMed: 23811844]

Hoogland TM, de Gruijl JR, Witter L, Canto CB, & de Zeeuw CI (2015). Role of synchronous activation of cerebellar Purkinje cell ensembles in multi-joint movement control. Current Biology, 25(9), 1157–1165. 10.1016/j.cub.2015.03.009 [PubMed: 25843032]

Hoogland TM, Kuhn B, Göbel W, Huang W, Nakai J, Helmchen F, Flint J, & Wang SSH (2009). Radially expanding transglial calcium waves in the intact cerebellum. Proceedings of the National Academy of Sciences of the United States of America, 106(9), 3496–3501. 10.1073/pnas.0809269106 [PubMed: 19211787]

Hoshino H, & Kubota M (2014). Canavan disease: Clinical features and recent advances in research. Pediatrics International, 56(4), 477–483. 10.1111/ped.12422 [PubMed: 24977939]

Hoxha E, Tempia F, Lippiello P, & Miniaci MC (2016). Modulation, plasticity and pathophysiology of the parallel fiber-Purkinje cell synapse. Frontiers in Synaptic Neuroscience, 8, 35. [PubMed: 27857688]

Huang W, Wang H, Kekuda R, Fei YJ, Friedrich A, Wang J, Conway SJ, Cameron RS, Leibach FH, & Ganapathy V (2000). Transport of N-Acetylaspartate by the Na2-dependent high-affinity dicarboxylate transporter NaDC3 and its relevance to the expression of the transporter in the brain. J Pharmacol Exp Ther, 295, 392–403. [PubMed: 10992006]

Hull V, Wang Y, Burns T, Zhang S, Sternbach S, McDonough J, Guo F, & Pleasure D (2020). Antisense oligonucleotide reverses leukodystrophy in Canavan disease mice. Annals of Neurology, 87(3), 480–485. 10.1002/ana.25674 [PubMed: 31925837]

Iino M, Goto K, Kakegawa W, Okado H, Sudo M, Ishiuchi S, Miwa A, Takayasu Y, Saito I, Tsuzuki K, & Ozawa S (2001). Glia-synapse interaction through Ca2+-permeable AMPA receptors in Bergmann glia. Science, 292(5518), 926–929. 10.1126/science.1058827 [PubMed: 11340205]

Ishiuchi S, Tsuzuki K, Yamada N, Okado H, Miwa A, Kuromi H, Yokoo H, Nakazato Y, Sasaki T, & Ozawa S (2001). Extension of glial processes by activation of Ca2+-permeable AMPA receptor channels. Neuroreport, 12(4), 745–748. 10.1097/00001756-200103260-00026 [PubMed: 11277576]

Ito M (2002). Historical review of the significance of the cerebellum and the role of Purkinje cells in motor learning. Annals of the new York Academy of Sciences, 978(1), 273–288. 10.1111/j.1749-6632.2002.tb07574.x [PubMed: 12582060]

Ito M (2006). Cerebellar circuitry as a neuronal machine. Progress in Neurobiology, 78(3–5), 272–303. 10.1016/j.pneurobio.2006.02.006 [PubMed: 16759785]

Keinänen K, Wisden W, Sommer B, Werner P, Herb A, Verdoorn TA, Sakmann B, & Seeburg PH (1990). A family of AMPA-selective glutamate receptors. Science (New York, N.Y.), 249(4968), 556–560. 10.1126/science.2166337 [PubMed: 2166337]

Koeppen AH (2005). The pathogenesis of spinocerebellar ataxia. The Cerebellum, 4(1), 62–73. 10.1080/14734220510007950 [PubMed: 15895563]

Kolodziejczyk K, Hamilton NB, Wade A, Káradóttir R, & Attwell D (2009). The effect of N-acetyl-aspartyl-glutamate and N-acetyl-aspartate on white matter oligodendrocytes, brain: A. Journal of Neurology, 132(Pt 6), 1496–1508. 10.1093/brain/awp087 [PubMed: 19383832]

Kozareva V, Martin C, Osorno T, Rudolph S, Guo C, Vanderburg C, Nadaf N, Regev A, Regehr WG, & Macosko E (2021). A transcriptomic atlas of mouse cerebellar cortex comprehensively defines cell types. Nature, 598(7879), 214–219. 10.1038/s41586-021-03220-z [PubMed: 34616064]

Kuo S-H, Lin CY, Wang J, Sims PA, Pan MK, Liou JY, Lee D, Tate WJ, Kelly GC, Louis ED, & Faust PL (2017). Climbing fiber-Purkinje cell synaptic pathology in tremor and cerebellar degenerative diseases. Acta Neuropathologica, 133(1), 121–138. 10.1007/s00401-016-1626-1 [PubMed: 27704282]

Author Manuscript Author Manuscript Author Manuscript Author Manuscript

Lesslich HM, Klapal L, Wilke J, Haak A, & Dietzel ID (2022). Adjusting the neuron to astrocyte ratio with cytostatics in hippocampal cell cultures from postnatal rats: A comparison of cytarabino furanoside (AraC) and 5-fluoro-2'-deoxyuridine (FUdR). PLoS One, 17(3), e0265084. 10.1371/journal.pone.0265084 [PubMed: 35263366]

Lin C-Y, Louis ED, Faust PL, Koeppen AH, Vonsattel JP, & Kuo SH (2014). Abnormal climbing fibre-Purkinje cell synaptic connections in the essential tremor cerebellum, brain: A. Journal of Neurology, 137(Pt 12), 3149–3159. 10.1093/brain/awu281

Lin X, Antalffy B, Kang D, Orr HT, & Zoghbi HY (2000). Polyglutamine expansion down-regulates specific neuronal genes before pathologic changes in SCA1. Nature Neuroscience, 3(2), 157–163. 10.1038/72101 [PubMed: 10649571]

Lordkipanidze T, & Dunaevsky A (2005). Purkinje cell dendrites grow in alignment with Bergmann glia. Glia, 51(3), 229–234. 10.1002/glia.20200 [PubMed: 15800897]

Marcaggi P, Billups D, & Attwell D (2003). The role of glial glutamate transporters in maintaining the independent operation of juvenile mouse cerebellar parallel fibre synapses. The Journal of Physiology, 552(Pt 1), 89–107. 10.1113/jphysiol.2003.044263 [PubMed: 12878755]

Matalon R, Michals K, & Kaul R (1995). Canavan disease: From spongy degeneration to molecular analysis. The Journal of Pediatrics, 127(4), 511–517. 10.1016/s0022-3476(95)70105-2 [PubMed: 7562269]

Matalon R, Michals K, Sebesta D, Deanching M, Gashkoff P, Casanova J, Optiz JM, & Reynolds JF (1988). Aspartoacylase deficiency and N-acetylaspartic aciduria in patients with Canavan disease. American Journal of Medical Genetics, 29(2), 463–471. 10.1002/ajmg.1320290234 [PubMed: 3354621]

Matsui K, & Jahr CE (2004). Differential control of synaptic and ectopic vesicular release of glutamate. The Journal of Neuroscience, 24(41), 8932–8939. 10.1523/JNEUROSCI.2650-04.2004 [PubMed: 15483112]

Meldrum B, & Garthwaite J (1990). Excitatory amino acid neurotoxicity and neurodegenerative disease. Trends in Pharmacological Sciences, 11(9), 379–387. 10.1016/0165-6147(90)90184-a [PubMed: 2238094]

Mendes MI, Smith DEC, Pop A, Lennertz P, Fernandez Ojeda MR, Kanhai WA, van Dooren SJM, Anikster Y, Barić I, Boelen C, Campistol J, de Boer L, Kariminejad A, Kayserili H, Roubertie A, Verbruggen KT, Vianey-Saban C, Williams M, & Salomons GS (2017). Clinically distinct phenotypes of Canavan disease correlate with residual Aspartoacylase enzyme activity. Human Mutation, 38(5), 524–531. 10.1002/humu.23181 [PubMed: 28101991]

Miyazaki T, Yamasaki M, Hashimoto K, Kohda K, Yuzaki M, Shimamoto K, Tanaka K, Kano M, & Watanabe M (2017). Glutamate transporter GLAST controls synaptic wrapping by Bergmann glia and ensures proper wiring of Purkinje cells. Proceedings of the National Academy of Sciences of the United States of America, 114(28), 7438–7443. 10.1073/pnas.1617330114 [PubMed: 28655840]

Müller T, Möller T, Berger T, Schnitzer J, & Kettenmann H (1992). Calcium entry through Kainate receptors and resulting Potassium-Channel blockade in Bergmann glial cells. Science, 256(5063), 1563–1566. 10.1126/science.1317969 [PubMed: 1317969]

Müller T, Fritschy JM, Grosche J, Pratt GD, Möhler H, & Kettenmann H (1994). Developmental regulation of voltage-gated K + channel and GABAA receptor expression in Bergmann glial cells. The Journal of Neuroscience, 14(5 Pt 1), 2503–2514. 10.1523/JNEUROSCI.14-05-02503.1994 [PubMed: 8182424]

Müller T, Möller T, Neuhaus J, & Kettenmann H (1996). Electrical coupling among Bergmann glial cells and its modulation by glutamate receptor activation. Glia, 17(4), 274–284. [PubMed: 8856324]

Nedergaard M (1994). Direct signaling from astrocytes to neurons in cultures of mammalian brain cells. Science (New York, N.Y.), 263(5154), 1768–1771. 10.1126/science.8134839 [PubMed: 8134839]

Nimmerjahn A, Kirchhoff F, Kerr JND, & Helmchen F (2004). Sulforhodamine 101 as a specific marker of astroglia in the neocortex in vivo. Nature Methods, 1(1), 31–37. 10.1038/nmeth706 [PubMed: 15782150]

Author Manuscript Author Manuscript Author Manuscript Author Manuscript

Nimmerjahn A, Mukamel EA, & Schnitzer MJ (2009). Motor behavior activates Bergmann glial networks. Neuron, 62(3), 400–412. 10.1016/j.neuron.2009.03.019 [PubMed: 19447095]

Parpura V, Basarsky TA, Liu F, Jeftinija K, Jeftinija S, & Haydon PG (1994). Glutamate-mediated astrocyte-neuron signalling. Nature, 369(6483), 744–747. 10.1038/369744a0 [PubMed: 7911978]

Perkins EM, Clarkson YL, Sabatier N, Longhurst DM, Millward CP, Jack J, Toraiwa J, Watanabe M, Rothstein JD, Lyndon AR, Wyllie DJA, Dutia MB, & Jackson M (2010). Loss of β-III Spectrin leads to Purkinje cell dysfunction recapitulating the behavior and neuropathology of spinocerebellar ataxia type 5 in humans. The Journal of Neuroscience, 30(14), 4857–4867. 10.1523/JNEUROSCI.6065-09.2010 [PubMed: 20371805]

Rakic P (1971). Neuron-glia relationship during granule cell migration in developing cerebellar cortex. A Golgi and electronmicroscopic study in Macacus rhesus. The Journal of Comparative Neurology, 141(3), 283–312. 10.1002/cne.901410303 [PubMed: 4101340]

Ramón y Cajal S (1909). Histologie du système nerveux de l'homme & des vertébrés. Ed. française rev. & mise à jour par l'auteur, tr. de l'espagnol par L (pp. 1–1012). Azoulay, Maloine. 10.5962/bhl.title.48637

Reichelt W, & Knöpfel T (2002). Glutamate uptake controls expression of a slow postsynaptic current mediated by mGluRs in cerebellar Purkinje cells. Journal of Neurophysiology, 87(4), 1974–1980. 10.1152/jn.00704.2001 [PubMed: 11929916]

Riquelme R, Miralles CP, & De Blas AL (2002). Bergmann glia GABA(a) receptors concentrate on the glial processes that wrap inhibitory synapses. The Journal of Neuroscience, 22(24), 10720–10730. 10.1523/JNEUROSCI.22-24-10720.2002 [PubMed: 12486165]

Rothstein JD, Dykes-Hoberg M, Pardo CA, Bristol LA, Jin L, Kuncl RW, Kanai Y, Hediger MA, Wang Y, Schielke JP, & Welty DF (1996). Knockout of glutamate transporters reveals a major role for astroglial transport in excitotoxicity and clearance of glutamate. Neuron, 16(3), 675–686. 10.1016/s0896-6273(00)80086-0 [PubMed: 8785064]

Rothstein JD, Martin L, Levey AI, Dykes-Hoberg M, Jin L, Wu D, Nash N, & Kuncl RW (1994). Localization of neuronal and glial glutamate transporters. Neuron, 13(3), 713–725. 10.1016/0896-6273(94)90038-8 [PubMed: 7917301]

Saab AS, Neumeyer A, Jahn HM, Cupido A, Šimek AAM, Boele HJ, Scheller A, le Meur K, Götz M, Monyer H, Sprengel R, Rubio ME, Deitmer JW, de Zeeuw CI, & Kirchhoff F (2012). Bergmann glial AMPA receptors are required for fine motor coordination. Science, 337(6095), 749–753. 10.1126/science.1221140 [PubMed: 22767895]

Sager TN, Thomsen C, Valsborg JS, Laursen H, & Hansen AJ (1999). Astroglia contain a specific transport mechanism for N-acetyl-L-aspartate. Journal of Neurochemistry, 73(2), 807–811. 10.1046/j.1471-4159.1999.0730807.x [PubMed: 10428079]

Sasaki T, Beppu K, Tanaka KF, Fukazawa Y, Shigemoto R, & Matsui K (2012). Application of an optogenetic byway for perturbing neuronal activity via glial photostimulation. Proceedings of the National Academy of Sciences of the United States of America, 109(50), 20720–20725. 10.1073/pnas.1213458109 [PubMed: 23185019]

Shigetomi E, Patel S, & Khakh BS (2016). Probing the complexities of astrocyte calcium signaling. Trends in Cell Biology, 26(4), 300–312. 10.1016/j.tcb.2016.01.003 [PubMed: 26896246]

Shiwaku H, Yagishita S, Eishi Y, & Okazawa H (2013). Bergmann glia are reduced in spinocerebellar ataxia type 1. Neuroreport, 24(11), 620–625. 10.1097/WNR.0b013e32836347b7 [PubMed: 23778076]

Siegel A, Reichenbach A, Hanke S, Senitz D, Brauer K, & Smith TG Jr. (1991). Comparative morphometry of Bergmann glial (Golgi epithelial) cells: A Golgi study. Anatomy and Embryology, 183(6), 605–612. 10.1007/BF00187909 [PubMed: 1897747]

Sjöbeck M, & Englund E (2001). Alzheimer's disease and the cerebellum: A morphologic study on neuronal and glial changes. Dementia and Geriatric Cognitive Disorders, 12(3), 211–218. 10.1159/000051260 [PubMed: 11244215]

Smeets CJLM, Ma KY, Fisher SE, & Verbeek DS (2021). Cerebellar developmental deficits underlie neurodegenerative disorder spinocerebellar ataxia type 23. Brain Pathology (Zurich, Switzerland), 31(2), 239–252. 10.1111/bpa.12905 [PubMed: 33043513]

Author Manuscript Author Manuscript Author Manuscript Author Manuscript

Smith CIE, & Zain R (2019). Therapeutic oligonucleotides: State of the art. Annual Review of Pharmacology and Toxicology, 59(1), 605–630. 10.1146/annurev-pharmtox-010818-021050

Storck T, Schulte S, Hofmann K, & Stoffel W (1992). Structure, expression, and functional analysis of a Na(+)-dependent glutamate/aspartate transporter from rat brain. Proceedings of the National Academy of Sciences of the United States of America, 89(22), 10955–10959. 10.1073/pnas.89.22.10955 [PubMed: 1279699]

Takahashi M, Sarantis M, & Attwell D (1996). Postsynaptic glutamate uptake in rat cerebellar Purkinje cells. The Journal of Physiology, 497(Pt 2), 523–530. 10.1113/jphysiol.1996.sp021785 [PubMed: 8961192]

Traka M, Wollmann RL, Cerda SR, Dugas J, Barres BA, & Popko B (2008). Nur7 is a nonsense mutation in the mouse Aspartoacylase Gene that causes spongy degeneration of the CNS. Journal of Neuroscience, 28(45), 11537–11549. [PubMed: 18987190]

Vinueza Veloz MF, Zhou K, Bosman LWJ, Potters JW, Negrello M, Seepers RM, Strydis C, Koekkoek SKE, & de Zeeuw CI (2015). Cerebellar control of gait and interlimb coordination. Brain Structure and Function, 220(6), 3513–3536. 10.1007/s00429-014-0870-1 [PubMed: 25139623]

von Jonquieres G, Spencer ZHT, Rowlands BD, Klugmann CB, Bongers A, Harasta AE, Parley KE, Cederholm J, Teahan O, Pickford R, Delerue F, Ittner LM, Fröhlich D, McLean CA, Don AS, Schneider M, Housley GD, Rae CD, & Klugmann M (2018). Uncoupling N-acetylaspartate from brain pathology: Implications for Canavan disease gene therapy. Acta Neuropathologica, 135(1), 95–113. 10.1007/s00401-017-1784-9 [PubMed: 29116375]

Wang F, Xu Q, Wang W, Takano T, & Nedergaard M (2012). Bergmann glia modulate cerebellar Purkinje cell bistability via Ca2+-dependent K+ uptake. Proceedings of the National Academy of Sciences of the United States of America, 109(20), 7911–7916. 10.1073/pnas.1120380109 [PubMed: 22547829]

Wang Y, Hull V, Sternbach S, Popovich B, Burns T, McDonough J, Guo F, & Pleasure D (2021). Ablating the transporter sodium-dependent dicarboxylate transporter 3 prevents leukodystrophy in Canavan disease mice. Annals of Neurology, 90(5), 845–850. 10.1002/ana.26211 [PubMed: 34498299]

Wang Y, Zhang Y, Zhang S, Kim B, Hull VL, Xu J, Prabhu P, Gregory M, Martinez-Cerdeno V, Zhan X, Deng W, & Guo F (2021). PARP1-mediated PARylation activity is essential for oligodendroglial differentiation and CNS myelination. Cell Reports, 37(1), 109695. 10.1016/j.celrep.2021.109695 [PubMed: 34610310]

Watase K, Hashimoto K, Kano M, Yamada K, Watanabe M, Inoue Y, Okuyama S, Sakagawa T, Ogawa SI, Kawashima N, Hori S, Takimoto M, Wada K, & Tanaka K (1998). Motor discoordination and increased susceptibility to cerebellar injury in GLAST mutant mice. The European Journal of Neuroscience, 10(3), 976–988. 10.1046/j.1460-9568.1998.00108.x [PubMed: 9753165]

Yamada K, & Watanabe M (2002). Cytodifferentiation of bergmann glia and its relationship with purkinje cells. Anatomical Science International, 77(2), 94–108. 10.1046/j.0022-7722.2002.00021.x [PubMed: 12418089]

Zuo J, de Jager PL, Takahashi KA, Jiang W, Linden DJ, & Heintz N (1997). Neurodegeneration in lurcher mice caused by mutation in δ2 glutamate receptor gene. Nature, 388(6644), 769–773. 10.1038/42009 [PubMed: 9285588]

Author Manuscript Author Manuscript Author Manuscript Author Manuscript

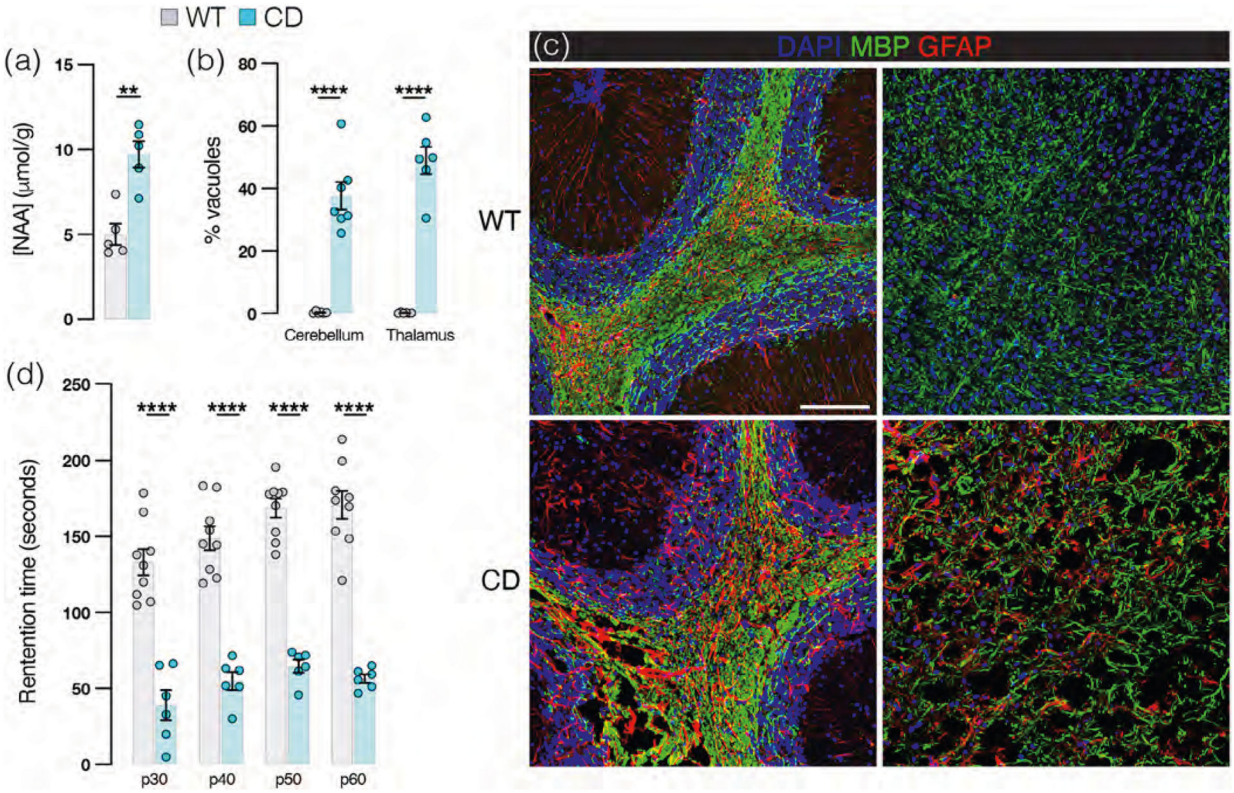

FIGURE 1.

Canavan disease mice present with ataxia and widespread brain vacuolation. (a) *N*-acetyl-L-aspartate brain concentration by HPLC (wild-type [WT]: 5.0 ± 0.64, Canavan disease (CD): 9.7 ± 0.76; $p = .0016$ by two-tailed Student's *t*-test). (b) Percent white matter vacuolation in adult murine cerebellum (WT: 0.3% ± 0.1%, CD: 37.7% ± 4.4%) and thalamus (WT: 0.2% ± 0.1%, CD: 48.9% ± 4.4%). $p < .0001$ by two-tailed Student's *t*-test for both. (c) Representative tissue sections from adult WT (top panel) and CD (bottom panel) mouse cerebellum (left panels) and thalamus (right panels) immunolabeled with antibodies against myelin marker MBP (myelin basic protein; green), astrocyte marker GFAP (glial fibrillary acidic protein; red) and counterstained with DAPI (blue). Scale bar = 50 μm. (d) Rotarod retention times in seconds(s): p30: WT: 133 ± 9, CD: 39 ± 10; p40: WT: 149 ± 8, CD: 55 ± 6; at p50 WT: 169 ± 6, CD: 65 ± 4; and p60 WT: 171 ± 9, CD: 57 ± 3. $p < .0001$ for all comparisons by two-tailed Student's *t*-test. (For all graphs: WT = gray and CD = blue. Data points represent averages for individual mice. Values reported are means (column height) ± SEMs (error bars). $^{**}p < .01$,$^{****}p < .0001$).

Author Manuscript
Author Manuscript
Author Manuscript
Author Manuscript

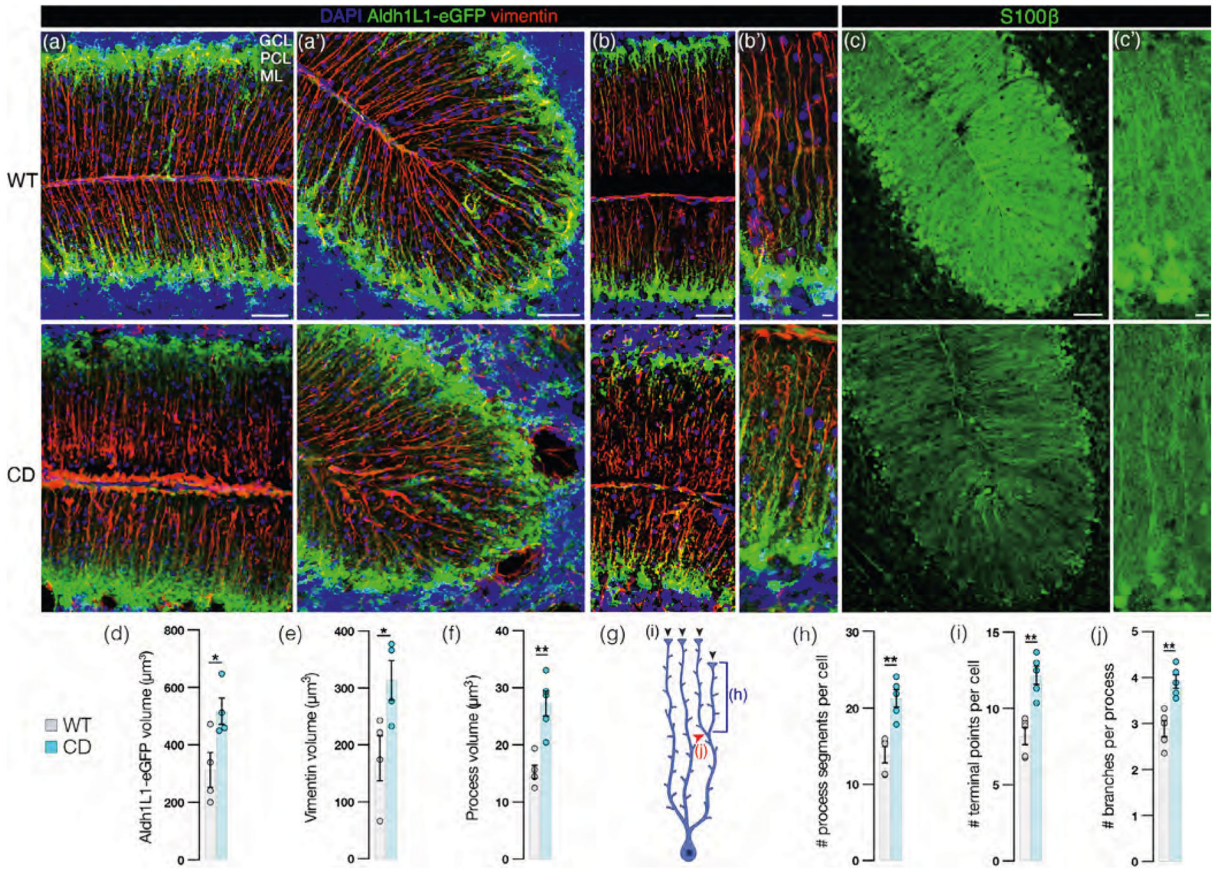

FIGURE 2.

Bergman glia exhibit discontinuous, swollen processes and irregular somatic morphology and position in Canavan disease (CD) mice. (a,b) Representative confocal images of the cerebellum from p60 wild-type (WT; top panel) and CD (bottom panel) transgenic Aldh1L1-eGFP mice, coimmunolabeled with Bergmann glia (BG) cytoskeletal marker vimentin (red) and DAPI (blue). (a,a') 30 μ z-stack images (scale bar = 50 μ). (b) 10 μ z-stack images (scale bar = 50 μ). (b') High power view of (b'; scale bar = 10 μ). (c) Cerebellar sections from p60 WT (top panel) and CD (bottom panel) mice immunostained with pan-astrocyte marker S100β (green; scale bar = 50 μm). (c') Higher power view of (c). (scale bar = 10 μm). (d) Average Aldh1L1-eGFP volume (μm^3) per BG cell: WT: 313.3 ± 60.6, CD: 517.2 ± 45.6. $p = .0361$ by two-tailed Student's *t*-test. (e) Average total vimentin volume (μm^3) per BG cell: WT: 176.5 ± 39.4, CD: 313.4 ± 35.0. $p = .0408$ by two-tailed Student's *t*-test. (f) Vimentin+ process volume (μm^3): WT: 15.3 ± 1.1, CD: 27.2 ± 2.1; $p = .0048$), (g) schematic depicting BG process specific features quantified by vimentin signal and reported in (h–j): (h) Number of process segments: WT: 13.9 ± 1.1, CD: 21.3 ± 1.1; $p = .0056$), (i) Number of process branches (WT: 2.9 ± 0.2, CD: 3.9 ± 0.1; $p = .0076$). (j) Number of terminal points (WT: 8.2 ± 0.6, CD: 12.2 ± 0.6; $p = .0052$). *p* values for f, h, i, j by 2-tailed Student's *t*-tests with Bonferroni correction for multiple comparisons. For all graphs: WT = gray and CD = blue. Data points represent averages for individual mice. Values reported are means (column height) ± SEMs (error bars). *$p < .05$; **$p < .01$). GCL, granule cell layer; ML, molecular layer; PCL, Purkinje cell layer.

Author Manuscript Author Manuscript Author Manuscript Author Manuscript

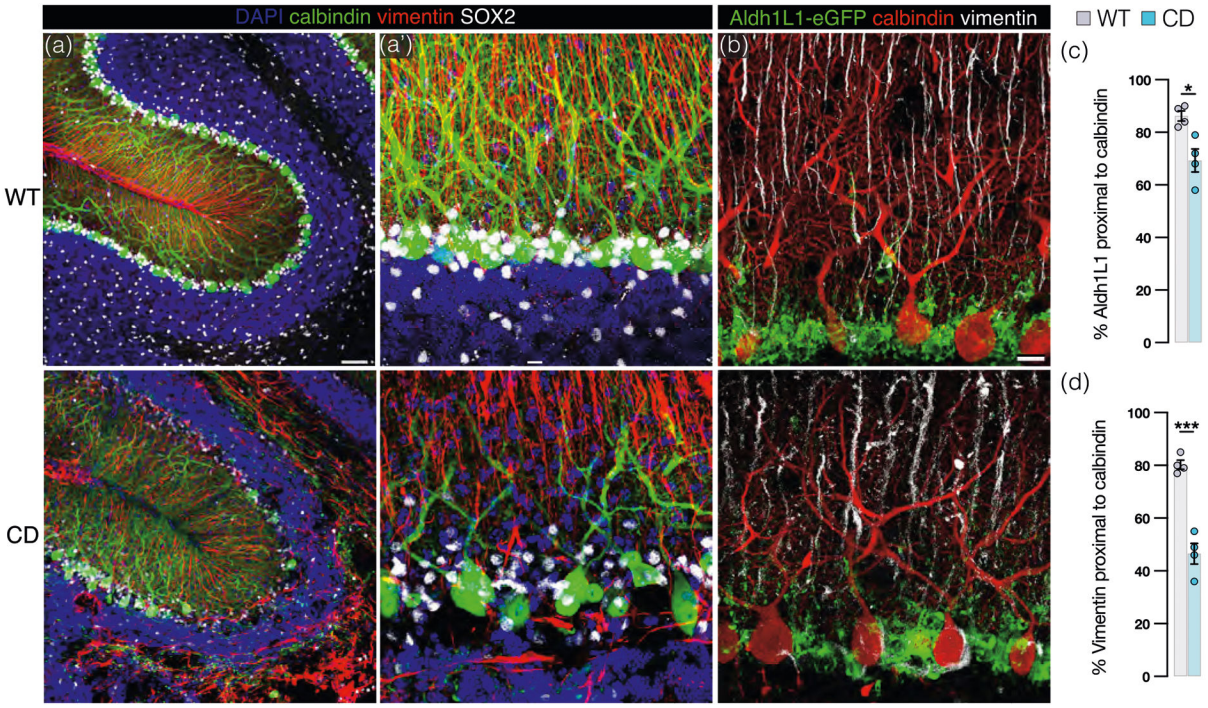

FIGURE 3.

Bergmann glia (BG)–Purkinje cell (PC) interactions are disrupted in Canavan disease (CD) mice. (a) Representative confocal images (30 μ z-stack) of cerebellar sections from adult wild-type (WT; top panel) and CD (bottom panel) mice immunolabeled with PC marker calbindin (green) and BG markers vimentin (cytoskeletal, red), SOX2 (somatic, white) counterstained with DAPI (blue; scale bar = 50 μm). High power view shown in (a'; scale bar = 10 μm). (b) 4 μ z-stack confocal images from Aldh1L1-eGFP+ (green) WT (top panel) and CD (bottom panel) mice costained with calbindin (red) and vimentin (white; scale bar = 10 μm). (c) Percent of BG marker Aldh1L1-eGFP within 1 μ proximity of PC marker calbindin in CD (69.25 ± 4.4) and WT (86.2 ± 1.9) mice ($p = .0121$ by two-tailed Student's *t*-test). (d) Percent of BG process marker vimentin within 1 μ proximity of PC marker calbindin in CD (46.5 ± 4.0) and WT (80.3 ± 1.7) mice ($p = .0002$ by two-tailed student's *t*-test). (For all graphs: WT = gray and CD = blue. Data points represent averages for individual mice. Values reported are means (column height) ± SEMs (error bars). *$p <$ .05, ***$p <$ .001).

Author Manuscript Author Manuscript Author Manuscript Author Manuscript

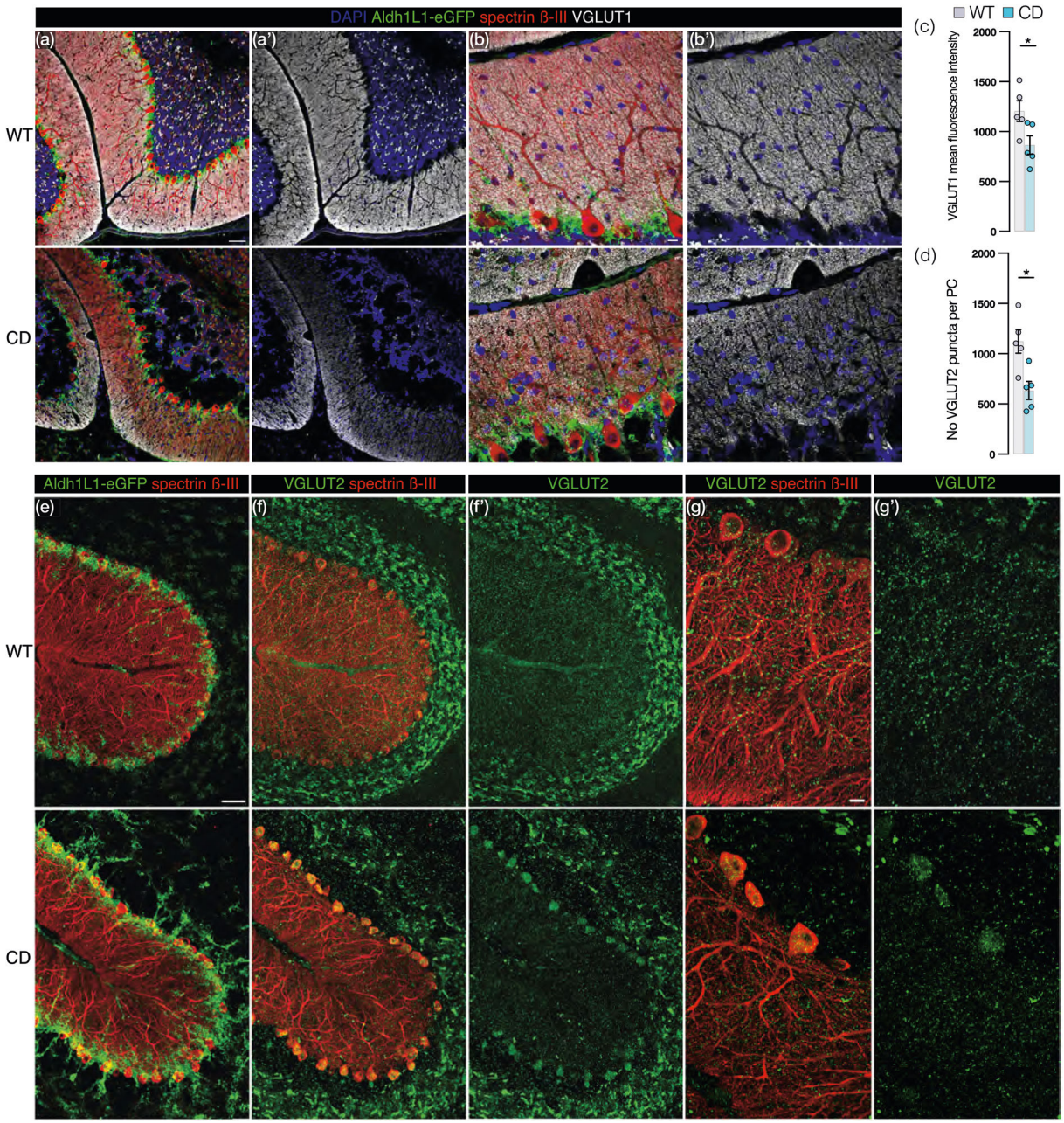

FIGURE 4.

Loss of parallel fiber (PF)- and climbing fiber-Purkinje cell (PC) synapses in Canavan disease (CD) mice. (a) Representative images from adult wild-type (WT; top panel) and CD (bottom panel) Aldh1L1-eGFP+ (green) mice immunostained with PC marker Spectrin β-III (red), PF–PC synaptic marker vesicular glutamate transporter 1 (VGLUT1; white) and DAPI (blue) with VGLUT1 and DAPI in isolation in (a'; scale bar = 50 μm). (b) High power images of (a), VGLUT1 and DAPI isolated in (b'; scale bar = 10 μm). (c) Mean fluorescence intensity of VGLUT1 signal in the molecular layer in CD (865 ± 92, blue) and WT (1206 ± 104) mice (p = .0397 by two-tailed student's t-test). (d) Average number of VGLUT2+ puncta per PC in CD (635 ± 89) and WT (1123 ± 117) mice (p = .0106 by

Author Manuscript Author Manuscript Author Manuscript Author Manuscript

two-tailed student's *t*-test). (e,f) Low power images (scale bar: 50 μm) from Aldh1L1-eGFP+ WT (top panel) and CD (bottom panel) mice: (e) Aldh1L1-eGFP (green) and spectrin β-III (red). (f) CF–PC synapse marker VGLUT2 (green) and spectrin β-III (red). (f') VGLUT2 (green) signal isolated. (g) High power view (scale bar = 10 μm) of (f), VGLUT2 (green) and spectrin β-III (red). (g') VGLUT2 (green) signal isolated. (For all graphs: WT = gray and CD = blue. Data points represents averages for individual mice. Values reported are means (column height) ± SEMs (error bars). *$p < .05$; **$p < .01$).

Author Manuscript Author Manuscript Author Manuscript Author Manuscript

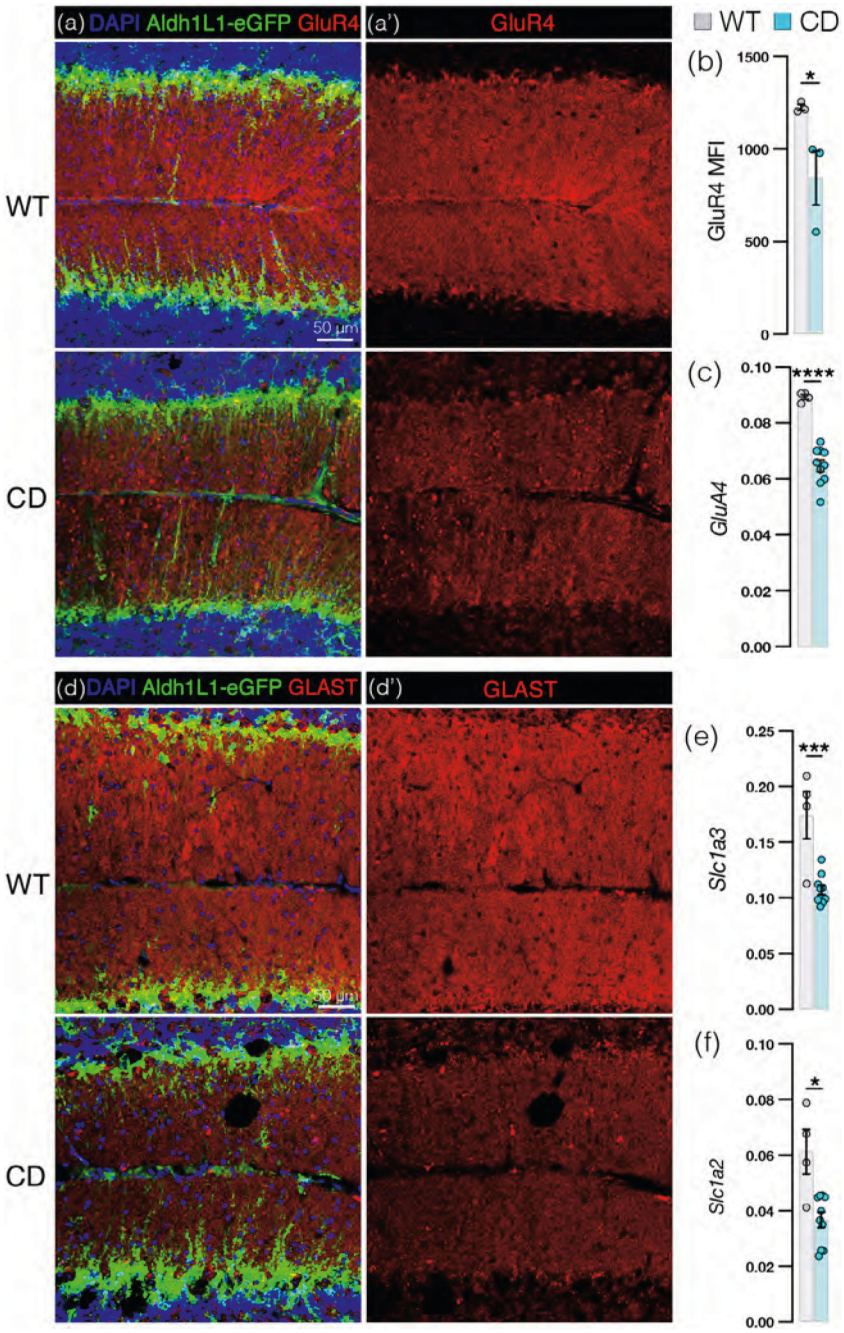

FIGURE 5.

Bergmann glia (BG) exhibit a loss of Ca^{2+}-permeable AMPARs and glutamate transporters in Canavan disease (CD) mice. (a) Representative cerebellar sections from adult wild-type (WT; top panel) and CD (lower panel) Aldh1L1-eGFP+ (green) mice immunostained for Ca^{2+}-permeable AMPAR subunit GluR4 (red) and counterstained with DAPI (blue) with GluR4 signal isolated in (a'; scale bar = 50 μm). (b) Mean fluorescence intensity of GluR4 in molecular layer of WT (1225 ± 16) and CD (843 ± 145) mice ($p = .047$ by one-way ANOVA, full comparisons shown in Figure 8b). (c) Relative *GluA4* mRNA abundance (normalized to *Hsp90*) by qRT-PCR in WT (0.089 ± 0.00087) and CD (0.064

Author Manuscript Author Manuscript Author Manuscript Author Manuscript

± 0.0021) mice ($p < .0001$ by one-way ANOVA, full comparisons shown in Figure 8c). (d) Representative cerebellar sections from WT (top panel) and CD (lower panel) Aldh1L1-eGFP+ (green) mice immunostained for glutamate transporter GLAST (red) and counterstained with DAPI (blue), with GLAST signal isolated in (d'; scale bar = 50 μm). (e) Relative *Slc1a3* (encodes GLAST) mRNA abundance (normalized to *Hsp90*) by qRT-PCR in WT (0.17 ± 0.021) and CD (0.11 ± 0.013) mice ($p = .0003$ by one-way ANOVA with post hoc Tukey's test, full comparisons shown in Figure 8e). (f) Relative *Slc1a2* (encodes GLT-1) mRNA abundance (normalized to Hsp90) by qRT-PCR in WT (0.061 ± 0.0080) and CD (0.37 ± 0.0028) mice ($p = .0221$ by one-way ANOVA, full comparisons shown in Figure 8f). (For all graphs: WT = gray and CD = blue. Data points represent individual mice. Values reported are means (column height) ± SEMs (error bars). *$p < .05$; ***$p < .001$; ****$p < .0001$).

Author Manuscript Author Manuscript Author Manuscript Author Manuscript

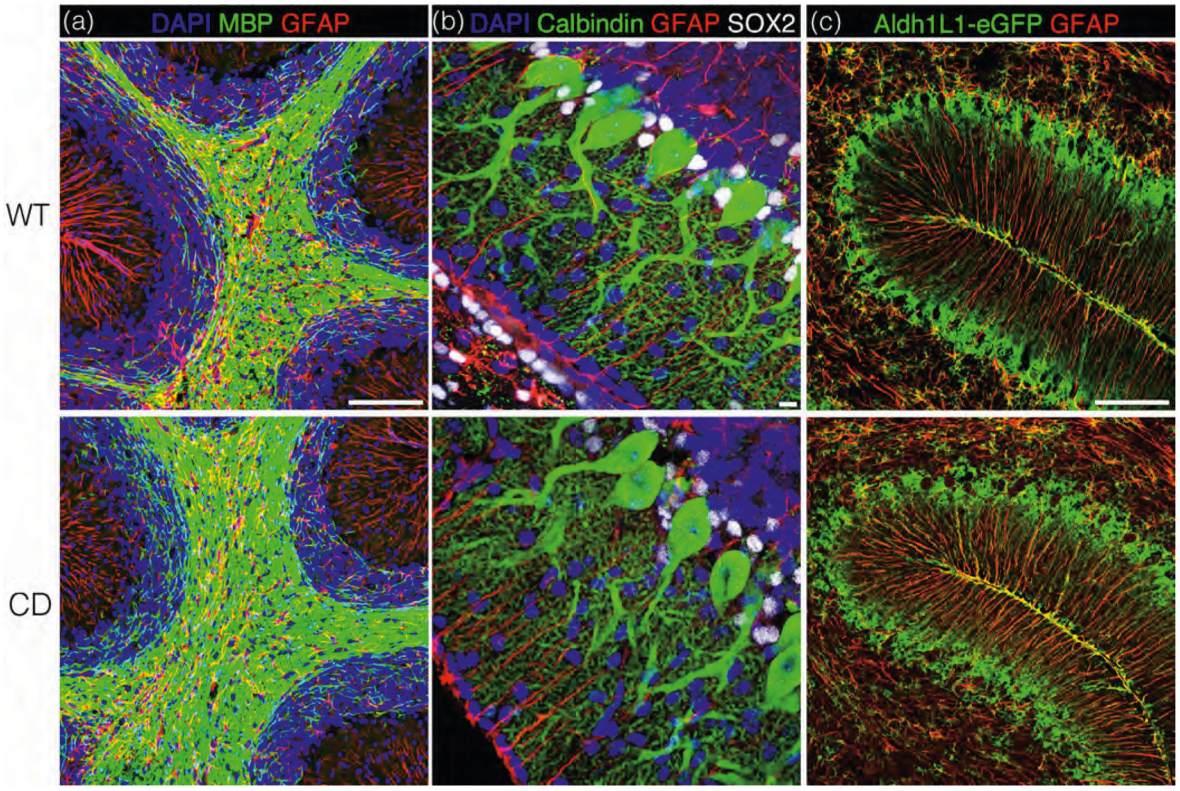

FIGURE 6.

Bergmann glia (BG) dysfunction predates cerebellar vacuolation and Purkinje cell damage in Canavan disease (CD) mice. Representative cerebellar sections from p15 wild-type (WT; top panel) and CD (bottom panel) mice. Panel (a) shows cerebellar white matter is immunostained myelin basic protein (MBP; green) and glial fibrillary acid protein (GFAP; red). High power views in panel (b) show Purkinje cells stained with calbindin (green) and Bergmann glia stained with GFAP (red) and SOX2 (white). Panel (c) shows transgenic Aldh1L1-eGFP expressing WT (top) and CD (bottom) mice stained with GFAP (red) to illuminate BG morphology. Scale bar = 50 μm in (a) and (c) and 10 μm in (b). Panels (a) and (b) have been counterstained with DAPI (blue).

Author Manuscript Author Manuscript Author Manuscript Author Manuscript

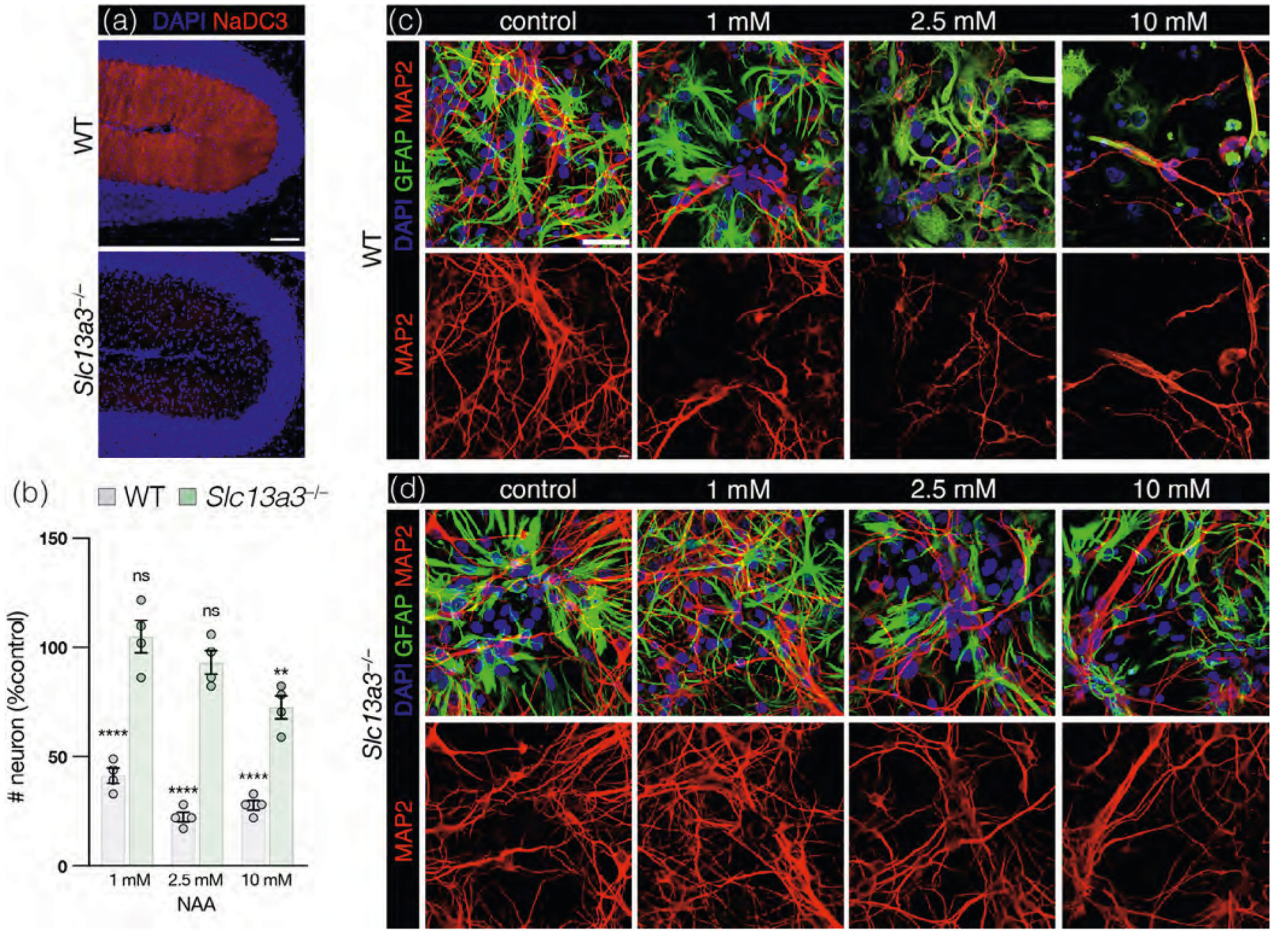

FIGURE 7.

Blocking astroglial uptake of NAA is neuroprotective in primary astrocyte-neuron cocultures. (a) Representative sections from wild-type (WT; top panel) and *Slc13a3*$^{-/-}$ (bottom panel) mice showing Bergmann glia expression of dicarboxylic acid transporter NaDC3 (encoded by *Slc13a3*; red) in the cerebellar molecular layer, counterstained with DAPI (blue). Scale bar = 50 μm. (b) Quantification of the number of MAP2+ neurons present in primary neonatal murine astroglia-neuron cocultures derived from WT mice = gray and cells derived from constitutive *Slc13a3* knockout mice (*Slc13a3*$^{-/-}$) = green. Cocultures were exposed to elevated *N*-acetyl-L-aspartate (NAA) for 48 h at the following concentrations: 1 mM (WT: 41.3% ± 3.4% of control, $p < .0001$; *Slc13a3*$^{-/-}$: 104.9% ± 7.4% of control, ns), 2.5 mM (WT: 22.3% ± 2.3% of control, $p < .0001$; *Slc13a3*$^{-/-}$: 93.1% ± 5.4% of control, ns), and 10 mM (WT: 27.8% ± 2.2% of control, <0.0001; *Slc13a3*$^{-/-}$: 72.5% ± 5.2% of control, $p = .0081$). Comparisons are against number of neurons in cocultures not treated with NAA, by one-way ANOVA with post hoc Tukey's test. WT and *Slc13a3*$^{-/-}$ control cultures were not significantly different. Representative images used for quantification are provided in (c) for WT cocultures and (d) for *Slc13a3*$^{-/-}$ cocultures where DAPI = blue, GFAP = green and MAP2 = red. Scale bar = 10 μm. Values reported are means (column height) ± SEMs (error bars). $^{**}p < .01$; $^{****}p < .0001$).

Author Manuscript Author Manuscript Author Manuscript Author Manuscript

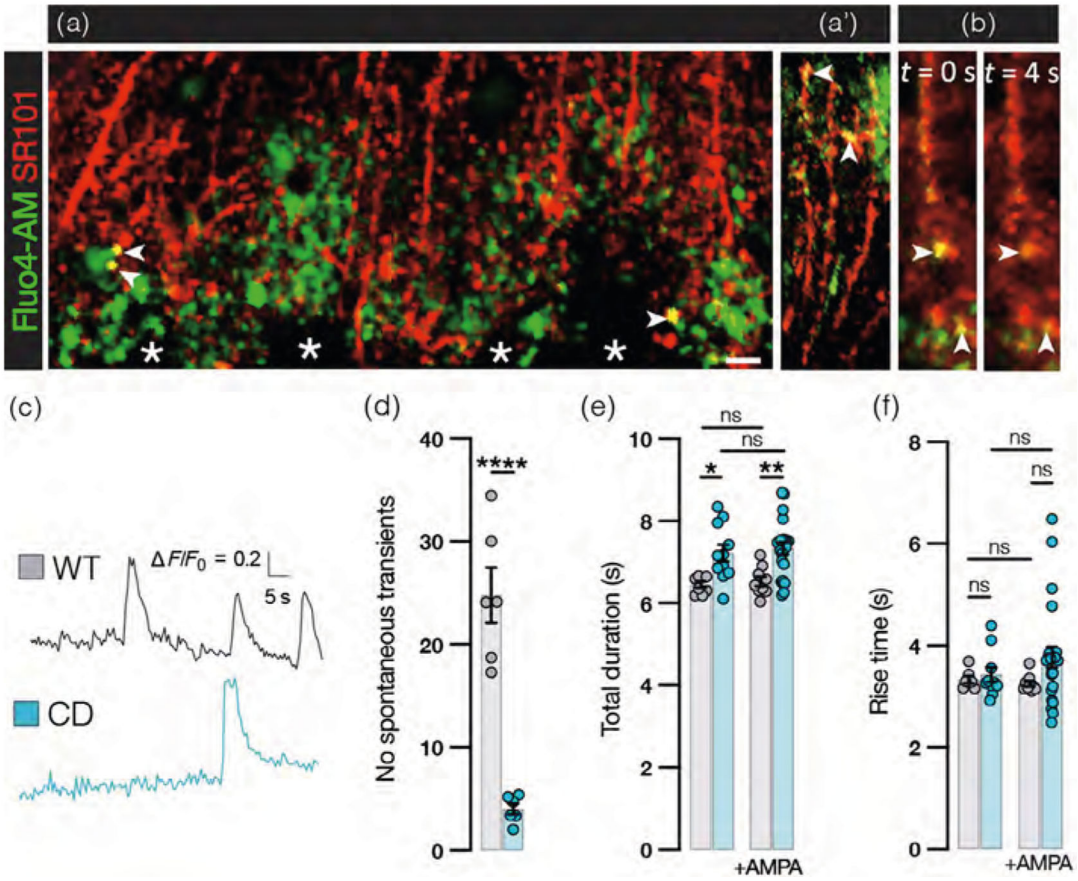

FIGURE 8.

Bergmann glia (BG) Ca^{2+} transients are less frequent and prolonged in Canavan disease (CD) mice. (a) Confocal image of single time frame of acute wild-type (WT) cerebellar slice loaded with Ca^{2+} sensitive dye Fluo4-AM (green) and labeled with the astrocyte-specific SR101 dye (red). Arrowheads point to spontaneous Ca^{2+} transients occurring in BG processes. Asterisks indicate Purkinje cell somata, not labeled by either dye. Scale bar = 10 μm. (a') Confocal image of Ca^{2+} transients (arrowheads) in distal BG processes near the pia. (b) Still capture from video at peak (left) of transients (arrowheads) and 4 seconds later (right). (c) Representative BG Ca^{2+} transient traces from WT (gray) and CD (blue) mice. (d) Frequency of spontaneous transients in BG per minute in 1000 μm^3 ROI. Each data point represents the average of 3 ROIs for 1 mouse (WT: 25.0 ± 2.7, CD: 4.0 ± 0.54; $p \leq .0001$ by two-tailed student's *t*-test). (e) Total duration (s) of spontaneous (WT: 6.5 ± 0.074, CD: 7.2 ± 0.21; $p = .0321$) and AMPA-evoked (WT: 6.5 ± 0.12, CD: 7.3 ± 0.15; $p = .0064$) transients (comparisons by one-way ANOVA with post hoc Tukey's test). (f) Rise time of spontaneous (WT:3.3 ± 0.070, CD: 3.4 ± 0.15, ns) and AMPA-evoked transients (WT: 3.3 ± 0.055, CD: 3.8 ± 0.21, ns; all comparisons by one-way ANOVA with post hoc Tukey's test). For (d,e), each data point represents the average of one microdomain over a 5-min recording window from $n = 4$ mice per group (for all graphs: WT = gray and CD = blue. Values reported are means (column height) ± SEMs (error bars). *$p < .05$; **$p < .01$; ****$p < .0001$).

Author Manuscript Author Manuscript Author Manuscript Author Manuscript

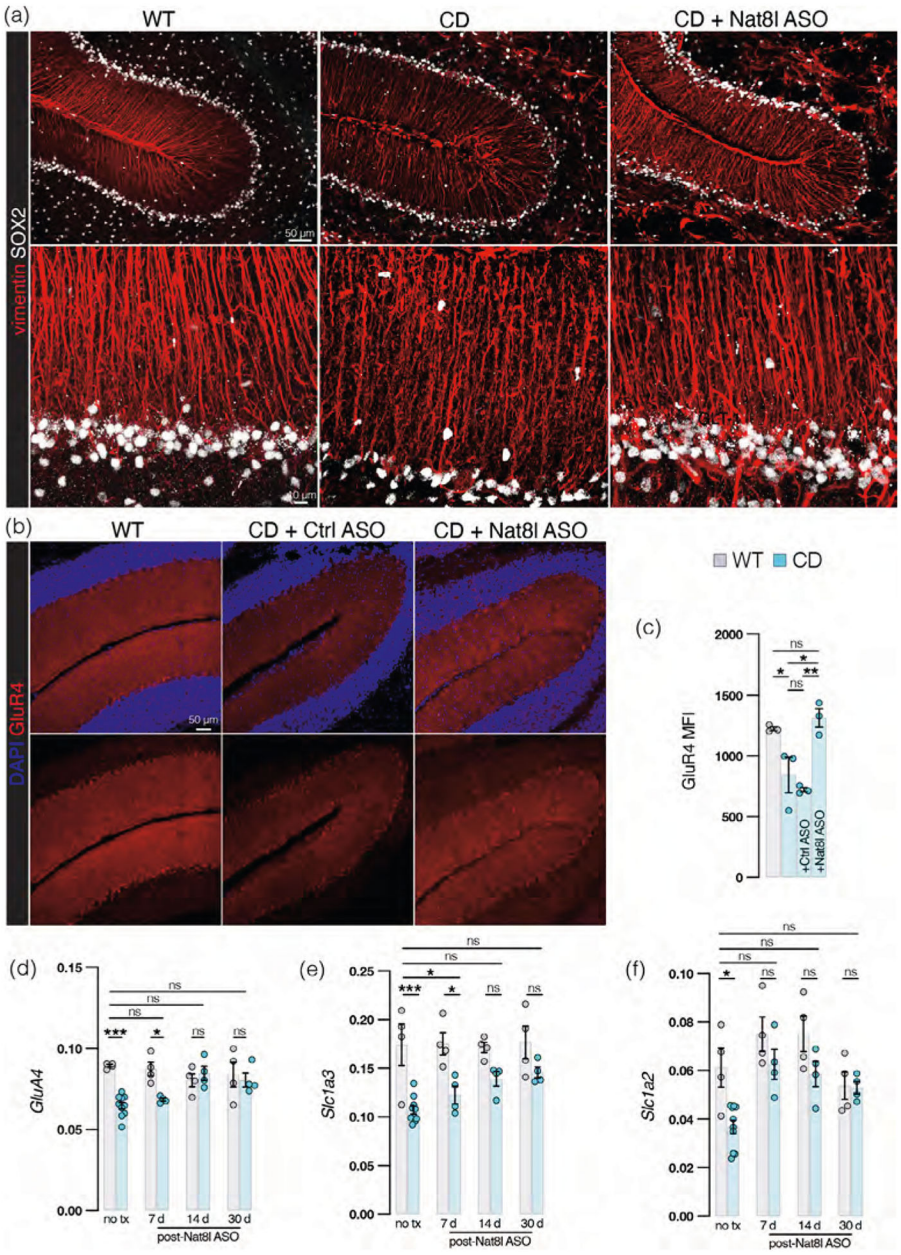

FIGURE 9.

Antisense oligonucleotide therapy repairs Bergmann glia (BG) irregularities observed in Canavan disease (CD) mice. (a) Representative cerebellar sections immunostained with BG process marker vimentin (red) and BG somatic marker SOX2 (white) from wild-type (WT; left), CD (middle) and CD mice 60 days after intracisternal injection of Nat8l antisense oligonucleotide (ASO; right) at low (top panel, scale bar = 50 μm) and high (bottom panel, scale bar = 10 μm) power. (b) Representative cerebellar sections immunostained with marker for Ca^{2+}-permeable AMPAR subunit GluR4 (red) and DAPI (blue) from WT BG process marker vimentin (red) and BG somatic marker SOX2 (white) from WT, CD, and Nat8l ASO-treated CD mice, 60 days posttreatment at low (top panel, scale bar = 50 μm) and high (bottom panel, scale bar = 10 μm) power. (c) Mean fluorescence intensity of GluR4

Author Manuscript Author Manuscript Author Manuscript Author Manuscript

in molecular layer of untreated WT (1225 ± 16) and CD (843 ± 145; same data shown in Figure 5b) mice as well as CD mice treated with control (ctrl) ASO (721 ± 18) and CD mice treated with Nat8l ASO (1314 ± 76) 60 days postadministration. *p* values by one-way ANOVA with post hoc Tukey's test: WT versus CD: $p = .0479$, CD + Nat8l ASO versus CD: $p = .0167$, CD + Nat8l ASO versus CD + Ctrl ASO: $p = .0044$. (d) Relative *GluA4* mRNA abundance (normalized to *Hsp90*) by qRT-PCR in untreated WT (0.089 ± 0.00087) and CD (0.064 ± 0.0021) mice ($p < .0001$, same data shown in Figure 5c) and Nat8l ASO-treated mice 7 days post (WT: 0.087 ± 0.0042, CD: 0.068 ± 0.00096, $p = .0443$), 14 days (WT: 0.080 ± 0.0040, CD: 0.085 ± 0.0044, ns), and 60 days post (WT: 0.084 ± 0.0076, CD: 0.081 ± 0.0043, ns) injection (comparisons by one-way ANOVA with post hoc Tukey's test). (e) Relative *Slc1a3* mRNA abundance (normalized to *Hsp90*) by qRT-PCR in untreated WT (0.17 ± 0.021) and CD (0.11 ± 0.013, blue) mice (same data presented in Figure 5e, $p = .0003$), 7 days posttreatment with Nat8l ASO in WT (0.18 ± 0.0041) and CD (0.12 ± 0.018) mice ($p = .0352$), 14 days posttreatment with Nat8l ASO in WT (0.17 ± 0.011) and CD (0.14 ± 0.015) mice (ns) and 30 days posttreatment with Nat8l ASO in WT and CD mice in WT (0.18 ± 0.0041) and CD (0.15 ± 0.011) mice (ns; comparisons by one-way ANOVA with post hoc Tukey's test). (f) Relative *Slc1a2* mRNA abundance (normalized to *Hsp90*) by qRT-PCR in WT (0.061 ± 0.0080) and CD (0.37 ± 0.0028) mice (same data presented in Figure 5f, $p = .0221$), 7 days posttreatment with Nat8l ASO in WT (0.075 ± 0.0071) and CD (0.063 ± 0.0062) mice (ns), 14 days posttreatment with Nat8l ASO in WT (0.075 ± 0.0073) and CD (0.059 ± 0.0052) mice (ns) and 30 days posttreatment with Nat8l ASO in WT and CD mice in WT (0.054 ± 0.0056) and CD (0.053 ± 0.0026) mice (ns; comparisons by one-way ANOVA with post hoc Tukey's test). (For all graphs: WT = gray and CD = blue, treatments specified. Values reported are means (column height) ± SEMs (error bars). $*p < .05$; $**p < .01$; $***p < .001$).

Author Manuscript Author Manuscript Author Manuscript Author Manuscript

Glia. Author manuscript; available in PMC 2023 December 01.

TABLE 1

Antibodies and Primers.

Antibody	**RRID**	**Concentration used**
calbindin	AB_868617	IHC 1:200
GFAP	AB_1074611 (Figures 1 and 6)	ICC/IHC 1:100
	AB_11212597 (Figure 7)	
GFP	AB_11181883	IHC 1:200
GLAST	AB_2811303	IHC 1:200
GluR4	AB_90711	IHC 1:300
MAP2	AB_2722660	ICC 1:200
MBP	AB_10655672	IHC 1:50
NaDC3	AB_2868533	IHC 1:200
SOX2	AB_10710406	IHC 1:20
Spectrin β-III	AB_2194518	IHC 1:200
S100β	AB_10983883	IHC 1:100
VGLUT1	AB_262185	IHC 1:200
VGLUT2	AB_1587626	IHC 1:200
vimentin	AB_10003206	IHC 1:1000

Gene name	**Forward primer sequence**	**Reverse primer sequence**	**Source**
Slc1a2	CAACGGAGGATATCAGTCTGC	TGTTGGGAGTCAATGGTGTC	Integrated DNA Technologies
Slc1a3	CAAGACACTGACACGCAAGGAC	CTTAACATCTTCCTTGGTGAGGC	
GluA4	GGGAGGTGACTCCAAGGACA	CCAGTGATGGATAACCTGGCT	
Hsp90	AAACAAGGAGATTTTCCTCCGC	CCGTCAGGCTCTCATATCGAAT	